# β- and δ-Al-Fe-Si intermetallic phase, their intergrowth and polytype formation

H. Becker[1,3], T. Bergh[2], P. E. Vullum[2], A. Leineweber[1], Y. Li[3]

[1]TU Bergakademie Freiberg, Institute of Materials Science, 09599 Freiberg, Germany

[2]Norwegian University of Science and Technology, Department of Physics, Trondheim, Norway

[3]Norwegian University of Science and Technology, Department of Materials Science and Engineering, Trondheim, Norway

## Abstract

Crystal structure characteristics of coexisting β and δ phase were investigated in a purely intermetallic Al-Fe-Si alloy and in plate-shaped intermetallic particles formed in a model secondary Al7.1Si1.2Fe0.3Mn alloy. The β- and the δ-Al-Fe-Si intermetallic phase are thermodynamic and crystallographic distinct phases despite some structural similarities. Nevertheless, both phases can appear severely intergrown within single plate-shaped particles after solidification of Fe-containing secondary Al-Si alloys under non-equilibrium conditions which is attributed to the good fit along the (001) planes of both phases. Thereby, few layers of the δ-like stacking sequences within the β phase can be considered as a typical planar defect of the β phase. The β phase exhibits polytype structures for which structural models have been formulated based on ordering of the constituting double layers being shifted by **a**/2 or **b**/2 displacements leading to 4 different double layer positions A, B, C, and D. An AB polytype with idealized *Acam* symmetry actually shows a monoclinic distortion towards *A*12/*a*1 symmetry. An ABCD polytype with idealized $I4_1/acd$ symmetry has been derived, too. Next to the ordered polytypes, stackings with non-periodic sequences of A, B, C and D double layers exist.

## Keywords

Intermetallics; metals and alloys; solidification; order-disorder effects; microstructure; crystal structure

## 1. Introduction

The β and δ phase form as plate-shaped intermetallic particles in secondary, Fe-containing Al-Si alloys during solidification [1- 9] and occur during bonding (or as a result of bonding) of Al-Si alloys to cast iron or steel [10, 11]. According to the Al-Fe-Si phase diagram [12], the β and δ phase are essentially stable phases. The β phase occurs at approx. the same Fe content, lower Si and higher Al contents, but approx. similar (Al+Si) molar fractions as the δ phase. Based on chemical composition analysis, the phases are called β-$Al_{4,5}FeSi$ [13- 16], β-$Al_5FeSi$ [17] or β-$Al_5Fe_2Si$ [18] and δ-$Al_3FeSi_2$ [9, 15, 19, 20] or δ-$Al_4FeSi_2$ [21].

For hypoeutectic secondary Al-Si alloys, in which undesired levels of Fe may have enriched during recycling, plate-shaped intermetallic particles are usually assigned to the β phase consistently with reported phase diagrams [12]. However, depending on the formation conditions, e.g. for higher cooling rates, the plates have been reported to be δ phase instead of β phase [6, 22]. Thereby, the intermetallic phases, especially within secondary Al-Si alloys, are often only identified based on their morphology and/or chemical composition [22-26]. Because of such apparently somewhat superficial

procedures, the correct phase identification of the plate-shaped intermetallic particles is sometimes doubted [9].

During previously conducted investigations on the formation of intermetallic particles in a secondary, Fe-containing Al-Si alloy [27], we have encountered significant backscatter electron contrast differences within the plate-shaped particles suggesting a multiphase character due to intergrowth of β and δ phase (not illustrated in the previous study [27]). Therefore, a clear distinction between the two phases is required for a thorough and correct investigation of the phase formation in presence of plate-shaped particles. This distinction requires also a clear knowledge of the crystal structures of the β and δ phase, which is, however, still under discussion [9, 13-21]. The crystal structures of the β and δ phase are closely related, consisting of the same basic constituent layers (Figure 1(a)). Furthermore, in the β phase, the ordered stacking of the layers can lead to superstructure formation [13, 15-17, 28, 29], which can be classified as polytypes [30-32]. However, a systematic analysis of the polytypes is still lacking.

The objective of the present study is to give detailed insight into the crystal structure characteristics of the β and δ phase where both phases are simultaneously present in plate-shaped intermetallic particles in a model secondary Al-Si alloy. The analysis of the particles is supported by investigation of an intermetallic alloy consisting predominantly of β and δ phase. In view of the structural (crystallographic) similarities, chemical composition and simultaneous presence of both phases in the same plate-shaped particles, the question in how far these phases are really that thermodynamically distinct as implied by the phase diagrams will be answered. The crystal structure of the β phase is reanalysed with respect to polytype formation and the symmetry of the polytypes. Experimental evidence for the simultaneous presence of different polytypes in the β phase is given. Regarding the closely related crystal structures, reasons for the variety of reported symmetries are discussed. Considerations on possible superstructures originating from ordering of Al and Si atoms are beyond the scope of the present paper.

## 2. Experimental details

### 2.1 Preparation of the alloys

Two alloys were studied in this work: a *secondary* Al-Fe-Mn-Si alloy and an *intermetallic* Al-Fe-Si alloy. The *secondary* Al-Fe-Mn-Si alloy is meant as model alloy to represent a secondary Fe- and Mn-containing Al-Si alloy containing pre-eutectically to eutectically solidified, plate-shaped intermetallic particles. It contains 91.4 at% Al, 7.1 at% Si, 1.2 at% Fe and 0.3 at% Mn. The *intermetallic* Al-Fe-Si alloy consists of 60.4 at% Al, 24.2 at% Si and 15.4 at% Fe and was meant to be located within the β + δ two-phase region [12] to support the analysis of the crystal structure. The alloys were melted in an electric arc furnace from Fe (AlfaAesar, pieces, 99.99% metals basis) and Al (AlfaAesar, slugs, 99.9999% metals basis), Si (AlfaAesar, pieces, 99.9999% metal basis) and Mn (AlfaAesar, pieces, 99.95% metal basis). Weighing of the ingots indicated no significant loss (<0.05%) of the weighted-in material.

During all subsequent heat treatments, the samples were put in $Al_2O_3$ crucibles (GTS - Gieß-Technische-Sonderkeramik GmbH & KG, 99.7%) which were encapsulated in fused silica tubes with argon atmosphere of normal pressure at target temperature. The intermetallic alloy was heat treated at 575°C for 645 h for homogenization. Afterwards, the material was milled by hand in an agate mortar for powder X-ray diffraction (P-XRD) analysis. For relief of cold-work, the powder was again heat treated at 575°C for 2 h and quenched in water keeping the powder inside the fused silica tube.

The secondary Al-Si alloy was fully remelted at 850°C and cooled in air, leading to a cooling rate of 1.4 K/s at 650°C.

### 2.2 Analysis

Microstructural investigations by scanning electron microscopy (SEM) including backscattered electron (BSE) contrast imaging and energy-dispersive X-ray spectrometry (EDS) were carried out on the polished cross sections of the solidified alloy samples (final stage: colloidal silica suspension; OP-S, Struers). A low-vacuum thermal field-emission gun (FEG) Zeiss Supra 55 Variable Pressure scanning electron microscope equipped with a Genesis EDS system and TEAM software (EDAX) was used. To determine average chemical compositions and the standard deviation, 6 to 10 EDS point measurements per phase were performed. Electron backscatter diffraction (EBSD) mapping was performed using a high resolution NORDIF EBSD detector applying the NORDIF 3.35 software for EBSD pattern acquisition and the OIM software (EDAX) for automated indexing. A FEG Zeiss LEO 1530 GEMINI equipped with a Nordlys II EBSD detector (Oxford Instruments) and HKL Channel5 software (Oxford instruments) was used for single EBSD pattern acquisition.

Thin lamellae were prepared by focused ion beam from the intermetallic plate-shaped particles in the secondary Al-Si alloy for investigation by transmission electron microscopy (TEM) including selected area electron diffraction (SAED) and high angle annular dark field (HAADF) imaging in scanning mode in order to derive local insight into the crystal and defect structures of the β and δ phase. A double Cs corrected coldFEG JEOL JEM-ARM200F was utilized. Simulation of SAED images was done using the software CrystalMaker®.

Powder-X-ray diffraction (P-XRD) was carried out to determine the crystal structures present in the intermetallic Al-Fe-Si alloy. A Bruker D8 diffractometer was employed working in Bragg-Brentano reflection geometry, which is equipped with a Co tube and using a quartz-crystal Johannson monochromator in the primary beam and a LYNXEYE position sensitive detector for recording the diffracted radiation. This allowed use of monochromatic Co-Kα1 radiation ($\lambda$ = 1.788985 Å). Small amount of the powder was sedimented on 510-cut Si “zero background” sample holders. The recorded diffraction-angles ranged from 18° to 90°. The P-XRD data was evaluated by using the software TOPAS [33, 34]. Rietveld refinements were conducted based on the fundamental parameter approach involving description of the instrumental profile based on an instrumental standard measurement, and allowing for consideration of sample-dependent line broadening by additional convolutions.

## 3. General considerations on the crystal structures

### 3.1. The layered crystal structures of the β and δ phase

The crystal structures of the β and δ phase as described in the literature are closely related. The β and δ phase can be described in terms of basic layers parallel to (001) as basic constituent. The basic layers consist of bicapped square antiprisms with a Fe atom in the center, 2 apical capping Al/Si atoms and 8 Al/Si atoms sharing common edges within the basic layers (Figure 1(a)). The average composition $Fe(Al,Si)_{8/2}(Al,Si)_2 = Fe(Al,Si)_6$ per basic layer results. The basis layer has layer symmetry *p*4/*nbm* [35]. In the β and δ phase the capping apical Al/Si atoms are shared to some extent with corresponding atoms from adjacent layers, or they can terminate the layer, leading generally to

compositions $Fe(Al,Si)_{8/2}(Al,Si)_{2-x}$ = $Fe(Al,Si)_{6-x}$ with the parameter *x* depending on the degree of condensation of the layers via the apical Al/Si atoms.

The δ phase consists of a successive sequence of fully condensed basic layers sharing all the cap atoms (Figure 1(b)) leading to an average composition $Fe(Al,Si)_{8/2}(Al,Si)_{2/2}$ = $Fe(Al,Si)_5$ per condensed basic layer. The unit cell contains two of the condensed basic layers being mirrored at $(002)_\delta$ [19, 20]. The δ phase is reported to exist in space group *I*4/*mcm* [19, 20] being isotypic to $GaPd_5$ [20], $Al_{2.5}Si_{2.5}Mn$ = $Mn(Al,Si)_5$ [20] and $Al_3FeGe_2$ = $Fe(Al,Ge)_5$ [36]. The presence of extra reflections, not expected for *I*4/*mcm* symmetry, in selected area electron diffraction (SAED) and convergent-beam electron diffraction (CBED) patterns were attributed to multiple scattering, planar defects causing symmetry reduction [9] or to a superstructure with orthorhombic *Pbcn* symmetry due to ordering of Al and Si atoms [19, 21] (see Table 1). In spite of the different reported symmetries, several authors consistently report that if Si or Ge is present in a phase with δ-phase like crystal structure alongside with Al, these atoms only occupy the corners of the square-antiprisms [19, 20, 36], i.e. the formula of the δ phase should actually read $Fe(Al,Si)_{8/2}Al_{2/2}$.

Whereas in the δ phase all apical capping atoms of the $Fe(Al,Si)_6$ basic layers are shared, in the β phase only two basic layers condense leading to apical capping atoms terminating the non-condensed sides of the two condensed layers. Thus, *double layers* with composition $(Al,Si)Fe(Al,Si)_{8/2}(Al,Si)_{2/2}$ $Fe(Al,Si)_{8/2}(Al,Si)$ = $Fe(Al,Si)_{5.5}$ are formed (Figure 1(c)). The double layers have a layer symmetry *p*4/*mbm* [35]. Such an idealized double layer can be stacked in different fashion along **c**. Although the β phase is always described with near tetragonal lattice parameters, further reported details vary, summarized as being: monoclinic [13-15] e.g. with space group *A*12/*a*1 [13, 14], orthorhombic [17, 18] or tetragonal [16, 17] and with lattice parameter *c* either around 20.8 Å [13, 14, 17, 18] or 41.6 Å [15-17]. The former lattice parameter corresponds to 2 double layers per unit cell ($c = 2c_0$), while the latter lattice parameter corresponds to 4 double layers per unit cell ($c = 4c_0$). The crystallographic information available in literature is summarized in Table 1.

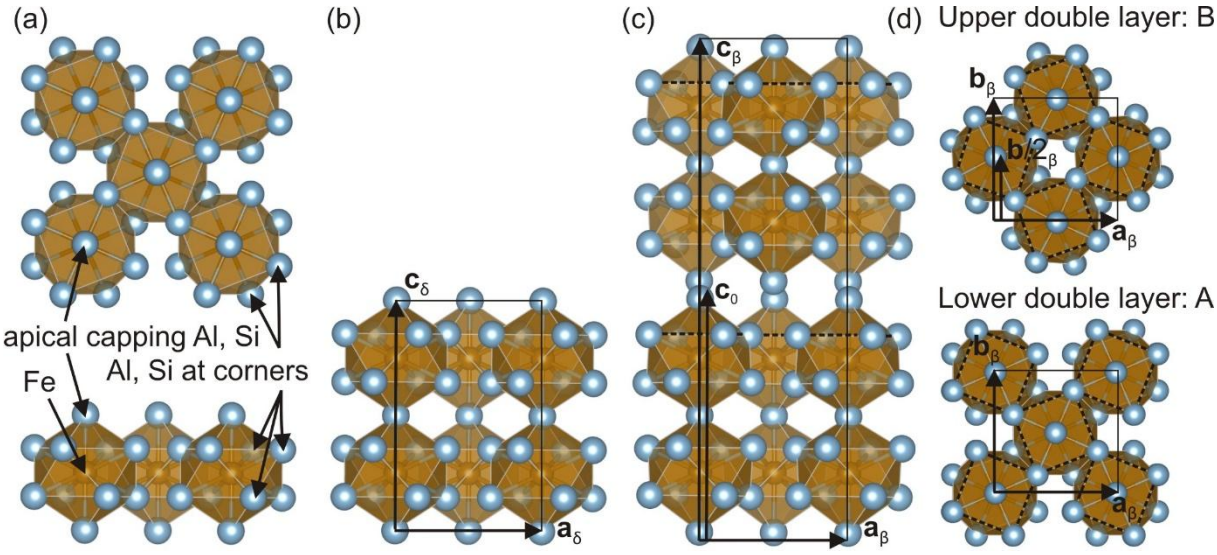


**Figure 1:** (a) A basic layer of bicapped square antiprisms $Fe(Al,Si)_6$ seen from the top and from the side. (b) The δ phase consists of a successive sequence of condensed basic layers sharing all the cap atoms leading to an average layer composition $Fe(Al,Si)_5$ [19]. The unit cell contains two basic layers being mirrored at $(002)_\delta$ planes. (c) The unit cell of the β phase consists of two double layers [13] which are periodically shifted by **b**/2 displacements and do not share cap atoms leading to an average layer composition $Fe(Al,Si)_{5.5}$ [13]. (d) Top view of the lower and upper double layer of the β

phase illustrating the **b**/2 displacement. Note that the top view of the lower double layer equals the top view of the δ phase.

**Table 1:** Review of crystallographic data on the β and δ phase. (SC-XRD: Single crystal XRD, P-XRD: Powder XRD, SAED: Selected area electron diffraction, CBED: Convergent-beam electron diffraction)

| Phase | Formula | Space group or crystal structure | | Lattice parameters | | | | Method | Ref |
|---|---|---|---|---|---|---|---|---|---|
| | | Symbol | number | *a* [Å] | *b* [Å] | *c* [Å] | *β* [°] | | |
| δ | $Al_3FeSi_2$ | *I*4/*mcm* | 140 | 6.061 | 6.061 | 9.525 | 90 | SC-XRD | 19 |
| | $Al_3FeSi_2$ | *I*4/*mcm* | 140 | 6.07 | 6.07 | 9.5 | 90 | P-XRD | 20 |
| | $Al_3FeSi_2$ | *Pbcn* | 60 | 6.061 | 6.061 | 9.525 | 90 | SC-XRD | 19 |
| | $Al_4FeSi_2$ | *I*4/*mcm* or *Pbcn* | 140 or 60 | 6.1455 | 6.1455 | 9.5093 | 90 | SAED | 21 |
| | $Al_3FeSi_2$ | *P*4/*mcm*[1] | | | | | | SAED, CBED | 9 |
| | $Al_3FeSi_2$ | Tetragonal | | 6.11 | 6.11 | 9.46 | 90 | XRD methods | 15 |
| β | $Al_{4.5}FeSi$ | *A*12/*a*1 | 15 | 6.1676 | 6.1661 | 20.8093 | 91 | P-XRD, SAED | 13 |
| | $Al_{4.5}FeSi$ | *A*12/*a*1 | 15 | 6.161 | 6.175 | 20.8130 | 90.42 | SAED, CBED | 14 |
| | $Al_5FeSi$ | *Amam*[2] | 63 | 6.18 | 6.20 | 20.8 | 90 | SAED, CBED | 17 |
| | $Al_5Fe_2Si$ | Orthorhombic *B*-centred | | 6.184 | 6.250 | 20.69 | 90 | CBED (XRD?) | 18 |
| | $Al_5FeSi$ | Tetragonal | | | | 41.6 | 90 | SAED, CBED | 17 |
| | $Al_{4.5}FeSi$ | Monoclinic | | 6.11 | 6.11 | 41.4 | 91 | XRD methods | 15 |
| | $Al_{4.5}FeSi$ | Tetragonal Laue group 4/*m* | | 6.18 | 6.18 | 42.5 | 90 | Laue, oscillation and Weissenberg photography | 16 |

[1]A corresponding space group does not exist [37]. It seems likely the reported consideration hint at the space group symbol $P4_2/mcm$, which is a subgroup of *I*4/*mcm*. However, neither an atomic model requiring break of the *I*4/*mcm* symmetry nor details about the reported planar faulting have been reported in [9].

[2]The orthorhombic space group *Amam* cannot correctly describe the currently considered atomic structure.

### 3.2 Polytypes of the β phase

The atomic structure of the β phase is based on **a**/2+$\mathbf{c}_0$ or **b**/2+$\mathbf{c}_0$ displacements of consecutive (ideally tetragonal) double layers being stacked along **c**, where **a** and **b** are the in-plane translation basis vectors of the double layer, introduced by Hansen et al. [13], and $\mathbf{c}_0$ is a vector perpendicular to the double layer with the length of the double layer distance $c_0$. For simplicity +$\mathbf{c}_0$ is omitted from the nomenclature during further descriptions in accordance with previously used nomenclature [13]. The **a**/2 and **b**/2 displacements lead to 4 different double layers positions, which can be called A, B, C and D (Figure 2(a)), analogous to the structures of $IrSn_4$ or $NiSn_4$ [38, 39]. Emanating from a double layer A, a B double layer is derived by a **b**/2 displacement, a D double layer is derived by an **a**/2 displacement and a C double layer results from a **b**/2+**a**/2 displacement. The different layers are illustrated in Figure 2(a) using the schematic version of what is shown in Figure 1. The assumption that an **a**/2 or **b**/2 displacement has to follow after each double layer is required to avoid that

terminated cap atoms become close to each other[1]. That allows an A or C double layer followed by a B or D double layer and vice versa. Thus, a stacking can be described by the sequence of **a**/2 or **b**/2 displacements or A, B, C and D double layer positions. Using the idealized tetragonal double layer as basic unit, idealized polytypes can be derived containing 2 or 4 double layers.

Pure stacking by periodic **b**/2 displacements of the double layers forms the **b**/2 - **b**/2 or AB polytype (Figure 2(b)). It has orthorhombic space group *Acam* (Table 2) with 2 double layers per unit cell; see Figure 3(a). A periodic **a**/2 displacement yields the same structure rotated by 90° around the stacking direction (space group *Bbcm*[2]). The reported monoclinic space group *A*12/*a*1 [13, 14] with $\beta$ close to 90° (Table 1) can be regarded as a result from some symmetry reduction based on the AB stacking sequence (only **b**/2 displacements) as *A*1/2*a*1 (*B*2/*b*11) is an equitranslatorial subgroup of order 2 of *Acam* (*Bbcm*).

The polytype containing 4 tetragonal double layers arises from a stacking sequence **b**/2 - **a**/2 - **b**/2 - **a**/2, similar to a stacking sequence discussed by [13]. This corresponds to a polytype including all 4 different double layer positions in the unit cell in an ABCD sequence (Figure 2(c)). The corresponding tetragonal space group can be identified as $I4_1/acd$ (Table 2). The structure is illustrated in Figure 3(b).

Diffraction patterns are quite similar for the polytypes. Certain reflections occur for all polytypes and for disordered cases of stacking. These reflections are called main (or fundamental) reflections. Some other reflections are characteristic for the particular polytype and are called polytype reflections. Main reflections have indices with $h + k = 2n$ (here and elsewhere, $n$ is an integer). The polytype reflections have indices with $h + k = 2n+1$. $l$ depends on the reflection conditions and is characteristic for each polytype. The reflection condition for the idealized orthorhombic AB polytype is $k + l = 2n$ and for the idealized tetragonal ABCD polytype is $h + k + l = 2n$. Additionally, polytype reflections 0$kl$ and $h0l$ are extinct for the symmetries of the ideal polytypes (Figure 3(a,b)), while their appearance indicates symmetry reduction present in the real polytype structures.

The two discussed polytypes for the β-phase structure represent specific cases of ordered sequences of the double layers (of which an infinite number can be imagined). Moreover, deviations from periodic stacking of double layer sequences will lead to diffuse streaking of intensity of polytype reflections along **c***. Superficial structure analysis, e.g. electron diffraction with [100]/[0$\bar{1}$0] and [110]/[1$\bar{1}$0] will miss the very characteristic (and anyway weak) polytype reflections and the characteristic diffuse scattering. In particular, in electron backscatter diffraction (EBSD) analysis, the distinction between the polytypes and assignment of the orientation of non-tetragonal polytypes (**a**/2 stacking vs. **b**/2 stacking) will be difficult or impossible in the course of routine measurements.[3] In order to perform robust EBSD analysis of the β phase alongside with distinction from the $\delta$ phase, a tetragonal structure with disordered stacking sequence is constructed (Figure 3(c)). That structure contains two $Fe(Al,Si)_{5.5}$ double layers per unit cell, which are themselves duplicate. The first double layer is at the A and C positions, and the second one is at the B and D positions, whereby, respectively the Fe and capping Al/Si positions coincide. Table 2 lists the atomic coordinates considering the $I4/mmm$ symmetry of this structure. The diffraction patterns from this structure feature only the main reflections but the polytype reflections are lacking (Figure 3(c)). Hence structure and orientation determination of β-phase like material on the basis of this structure model

[1] Condensation of apical atoms is allowed for displacement vectors of **0** and of **a**/2+**b**/2 of double layers. The former in relation with condensation of apical atoms occurs in the $\delta$ phase.

[2] The different symbols *Acam*, *Abma*, *Bbcm*, *Bmab*, *Ccmb* and *Cmc*a represent different choices of the axes. The standard setting would correspond to space group symbol *Cmce* which is equivalent to *Cmca* using the concept of double glide plane *e* [37].

[3] Such cases are discussed as systematic misindexing and pseudosymmetry problems in EBSD analysis [48].

will avoid complications related with inappropriate ability of an EBSD system to distinguish the different discussed polytypes and their orientations.

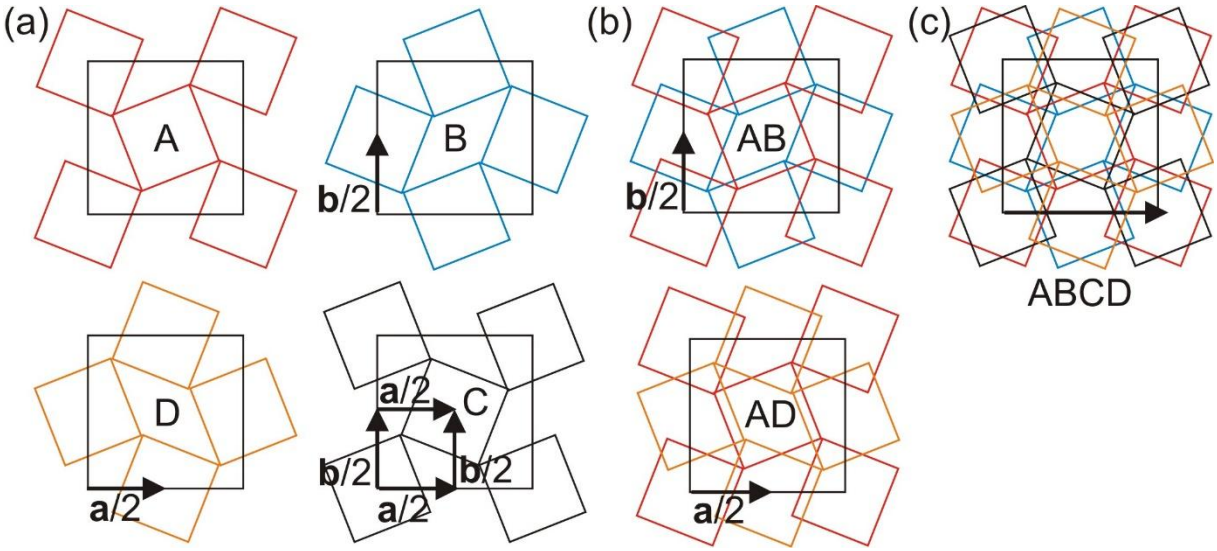


**Figure 2**: Schematic projection along **c** of double layers consisting of bicapped antiprism by squares sharing common edges as indicated by the dashed lines in Figure 1. (a) **b**/2 and **a**/2 displacements can lead to 4 different double layers A, B, C, D with respect to a basic double layer. (b) Periodic **b**/2 displacement illustrated by AB stacking sequence and **a**/2 displacement illustrated by AD stacking sequence. (c) Periodic **b**/2 - **a**/2 displacement corresponding to an ABCD stacking sequence.

**Table** 2: Space group and idealized atomic coordinates of the *Acam* and $I4_1/acd$ polytypes and the disordered *I*4/*mmm*. The atomic coordinates of $I4_1/acd$ polytype (choice of origin: 2) and the disordered *I*4/*mmm* are derived based on those of the idealized coordinates of the *Acam* space group and idealized lattice parameter $a = b = 6.168$ Å and $c = 20.809$ Å [13]. Partial occupation of Al and Si on Al sites with fractions 0.8182 Al and 0.1818 Si is assumed.

| Polytype sequence | | Space group | $a = b$ | $c$ | Site | Fractional coordinates | | | Fractional occupation |
|---|---|---|---|---|---|---|---|---|---|
| Displacement | Double layer | | [Å] | [Å] | | $x$ | $y$ | $z$ | |
| **b**/2 - **b**/2 | AB | *Acam* | 6.168 | 20.809 | Fe(1) | 0 | 0 | 0.887 | 1 |
| | | | | | Al(1) | 0.84784 | 0.34784 | 0.93 | 1 |
| | | | | | Al(2) | 0.84784 | 0.15216 | 0.34 | 1 |
| | | | | | Al(3) | 0 | 0 | 0 | 1 |
| | | | | | Al(4) | 0 | 0 | 0.23 | 1 |
| **b**/2 - **a**/2 - **b**/2 - **a**/2 | ABCD | $I4_1/acd$ | 6.168 | 41.618 | Fe(1) | 0 | 0.75 | 0.07 | 1 |
| | | | | | Al(1) | 0 | 0.75 | 0.125 | 1 |
| | | | | | Al(2) | 0.15216 | 0.09784 | 0.045 | 1 |
| | | | | | Al(3) | 0.15216 | 0.40216 | 0.09 | 1 |
| | | | | | Al(4) | 0 | 0.75 | 0.01 | 1 |
| (**b**/2,**a**/2) - (**b**/2,**a**/2) | (A,C) (B,D) | *I*4/*mmm* | 4.361 | 20.809 | Fe(1) | 0 | 0 | 0.3866 | 1 |
| | | | | | Al(1) | 0 | 0.69557 | 0.9354 | 0.5 |
| | | | | | Al(2) | 0 | 0.3044 | 0.15725 | 0.5 |
| | | | | | Al(3) | 0 | 0 | 0.27 | 1 |
| | | | | | Al(4) | 0 | 0 | 0.5 | 1 |

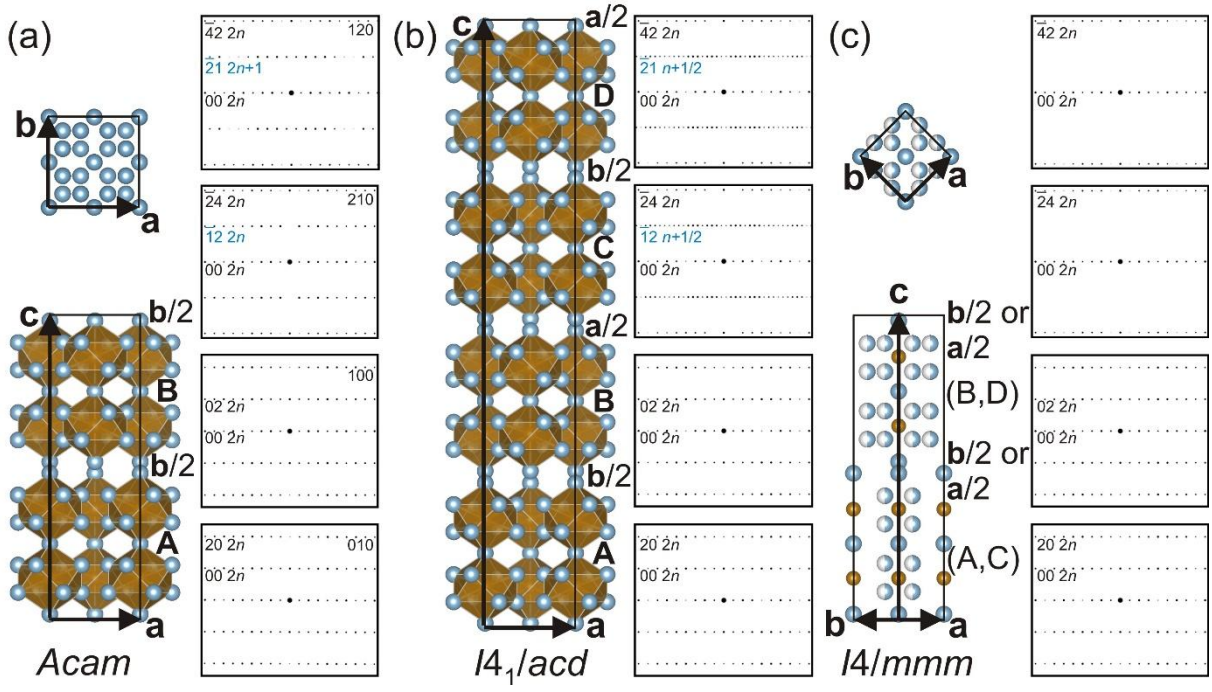


**Figure 3:** The β-phase structures described by (a) **b**/2 - **b**/2 or AB polytype (orthorhombic *Acam* structure), (b) **b**/2 - **a**/2 - **b**/2 - **a**/2 or ABCD polytype (tetragonal $I4_1/acd$ structure) and (b) a disordered structure (tetragonal *I*4/*mmm*) and the corresponding simulated electron diffraction images. The position A, B, C, D of the double layers and the displacement **a**/2 and **b**/2 are indicated. For illustrative purposes an origin shift has been applied to the fractional coordinates in Table 2. For comparison, indexing of polytypes is made with respect to the AB polytype. Note, that the simulated electron diffraction images are equivalent for incidence directions [120]/[210] and [100]/[010] for the tetragonal structures and can be more or less different for orthorhombic or lower symmetries. Rows of reflection indices shown in black indicate main reflections and in blue indicate polytype reflections.

## 4. Experimental results and discussion

### 4.1 Distinction of the β and δ phase occurring simultaneously in a microstructure

#### 4.1.1 Intermetallic alloy

It is easy to separately recognize β and δ phase in the homogenized intermetallic alloy as evidenced in the SEM by the clearly differing detected intensity upon BSE imaging due to differing chemical composition, visible as dark and light grains in Figure 4(a). Chemical compositions determined by EDS are shown in Table 3. The P-XRD data obtained from the intermetallic alloy powder (Figure 5) reveals presence of a multiphase mixture containing δ and β phase and a small amount of Si. Lattice parameters, atomic coordinates and site occupation for the δ phase with space group *I*4/*mcm* from [20] and Si ($Fd\bar{3}m$) from [40] are used as starting points for Rietveld refinement. In case of the β phase, both ordered polytypes discussed in section 3.2 are present. The incorporation of the polytypes of the β phase into the Rietveld refinement and the monoclinic character of one of the polytypes evident in the P-XRD pattern are discussed in detail in the section 4.2.4. Fractional coordinates and site occupation of the present phases were not refined. Lattice parameters *a* = 6.108

Å and $c$ = 9.491 Å for the δ phase and $a$ = 5.431 Å for Si result from the refinement. Coexistence of the β and δ phase in the long-term annealed intermetallic alloy confirms their thermodynamical distinctness in agreement to available phase diagrams [12] and as implemented e.g. in the thermodynamic TCAl4 database [41].

**Table 3:** Chemical compositions and standard deviations of the β and δ phase determined from EDS point measurements in the intermetallic alloy after homogenization, in the β plates in the secondary Al-Si alloy and for most often reported stoichiometries (compare to Table 1). The chemical composition of the β phase in the secondary Al-Si alloy corresponds to β plates without internal contrast variations in SEM/BSE image that indicate presence of δ phase. Deviations of summed chemical composition from 100 at% result from rounding.

| Phase | $x_{Al}$ [at.%] | $x_{Fe}$ [at.%] | $x_{Si}$ [at.%] | $x_{Mn}$ [at.%] | Comment |
|---|---|---|---|---|---|
| β | 67.5 ± 0.1 | 15.6 ± 0.1 | 16.8 ± 0.1 | - | Intermetallic Al-Fe-Si alloy |
| β plates | 67.6 ± 0.5 | 13.9 ± 0.2 | 17.8 ± 0.4 | 0.8 ± 0.1 | Secondary Al-Si alloy |
| β $Al_{4.5}FeSi$ | 69.2 | 15.4 | 15.4 | - | Reported composition |
| δ | 53.9 ± 0.1 | 17.1 ± 0.1 | 29.1 ± 0.1 | - | Intermetallic Al-Fe-Si alloy |
| δ $Al_3FeSi_2$ | 50.0 | 16.7 | 33.3 | - | Reported composition |

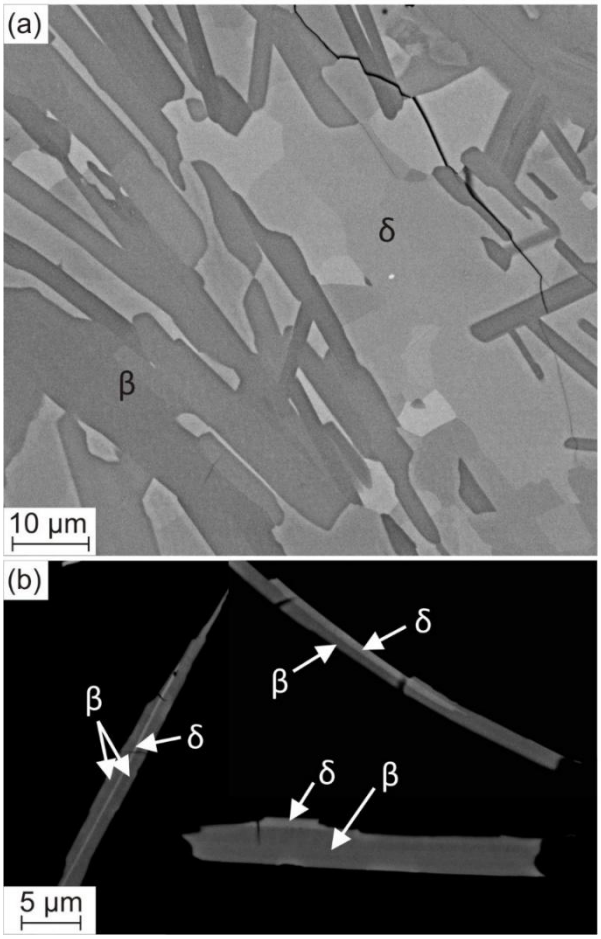


**Figure 4:** Appearance of the β and δ phase in the (a) intermetallic alloy and in the (b) secondary Al-Si alloy in BSE contrast. The Al matrix and Al-Si eutectic appear black in (b).

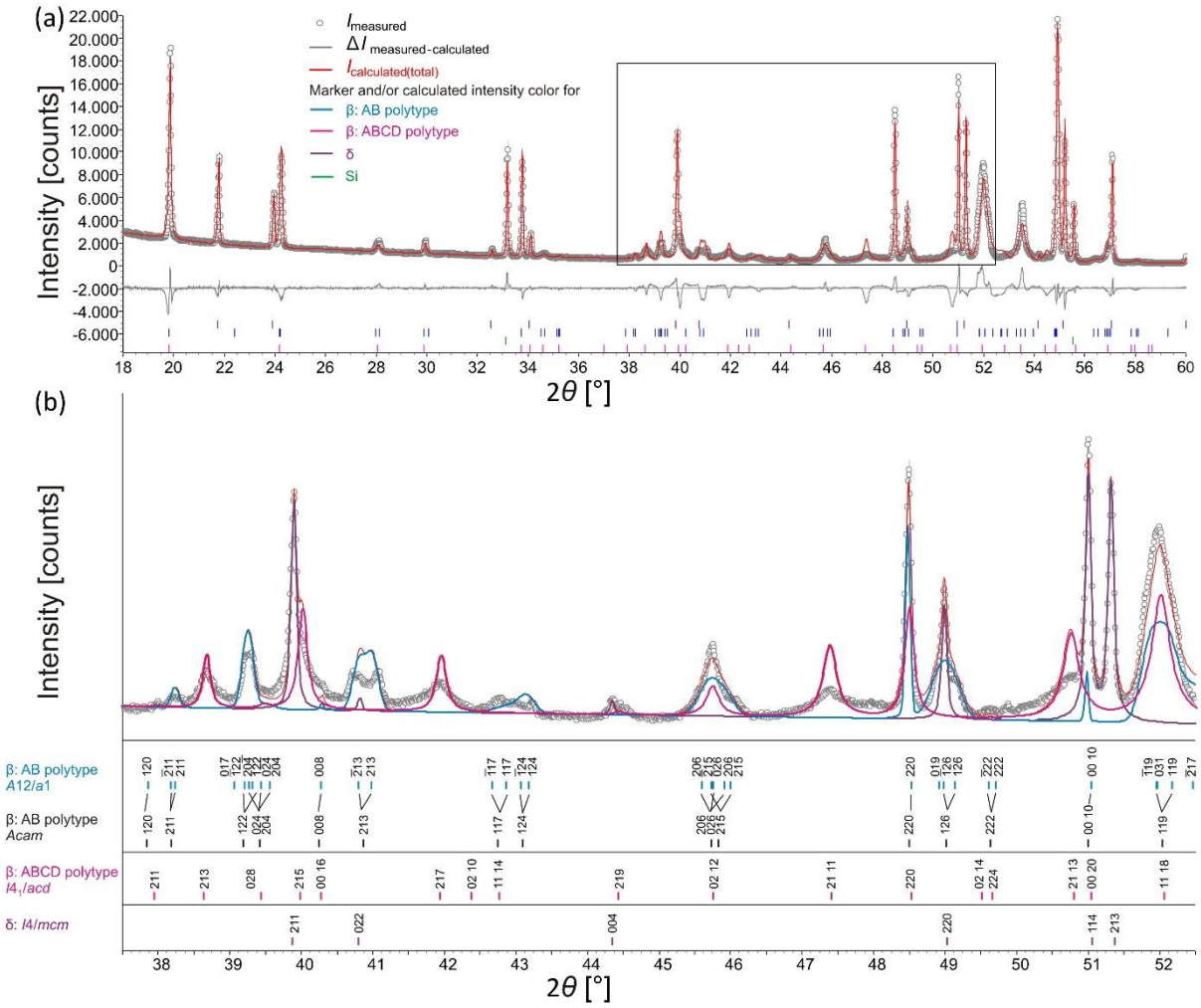


**Figure 5:** Result of a tentative Rietveld fit on the basis of powder-X-ray diffraction data (for more details see section 4.2.4) shown for 2$\theta$ part from (a) 18° to 60° and (b) magnified 2$\theta$ part from 37.5° to 52.5°. The reflection markers shown in the bottom refer to the AB and ABCD polytypes of the β phase with space groups *A*12/*a*1 and *I*4$_1$/*acd* and to the δ phase with space group *I*4/*mcm*. The colors of reflection markers are compatible with the color in the legend shown in (a). Additionally in (b) indices are shown for the orthorhombic *Acam* structure of the AB polytype highlighting the reflection splitting related to the monoclinic *A*12/*a*1 structure. For comparison, indexing of the ABCD polytype with *I*/2 corresponds to *I* = *n*+1/2 with respect to the AB polytype. Observed data points are shown with gray circles; the calculated profile is shown in red. The difference curve (observed–calculated intensity) is shown as gray line in the bottom of (a).

### 4.1.2 Plate-shaped intermetallic particles in the secondary Al-Si alloy

Plate-shaped intermetallic particles have formed in the secondary Al-Si alloy during solidification under non-equilibrium conditions. According to thermodynamic considerations using the ThermoCalc software [42] with the TCAl4 database [41], the δ phase should not form in the present secondary Al-Si alloy at any temperature under equilibrium conditions. Nevertheless, in the investigated sample, a quarter of the plates exhibits irregularly distributed stripes with similar dark and light gray contrast as in the intermetallic alloy when using the same SEM/BSE imaging conditions as for the intermetallic alloy (Figure 4(b)). These stripes indicate the mutual presence of the β and δ phase in the plates. Similar observations can be made for alloys of other Mn contents and also in Mn-free alloys (not shown). A comprehensive evaluation of the role of kinetics on the phase formation is beyond the

scope of the present paper and part of an ongoing investigation. The chemical composition of dark plates identified as β phase without light gray stripes is presented in Table 2. The chemical composition of the light gray stripes identified as δ phase has not been measured because these light gray stripes were too narrow to be resolved by EDS in SEM. The phase identification is confirmed by indexing of EBSD patterns from the dark and light gray stripes (Figure 6; see, however, also section 4.2.5).

Furthermore, bright field TEM imaging of a FIB lamella from a plate-shaped particle reveals the presence of rather contrast-free regions and regions with a high density of line-like contrast (Figure 7(a)). Selected area electron diffraction (SAED) from the rather contrast-free regions confirms the coexistence of β and δ phase in a single plate-shaped particle with the orientation relationship $(001)_\delta||(001)_\beta$ and $[100]_\delta||[100]_\beta$ (Figure 7(b)). The regions with a high density of line-like contrasts contain a complex sequence of β and δ layers. High-angle annular dark field (HAADF) imaging in incidence direction $[210]_\delta$ ($[210]_\beta$ or $[120]_\beta$) reveals double layers characteristic for the β phase and condensed basic layers characteristic for the δ phase (Figure 8(a)). The β and δ layers are distinguished by their relative difference in the *c* lattice parameter $\Delta c = (2c_\delta - c_\beta)/c_\beta = 0.085$ [13, 19]. Thus, in the example in Figure 8(a) three and seven successive condensed basic layers forming δ-like stacking sequences can be identified next to the double layers of the β phase. The non-periodic sequence of β and δ layers leads to diffuse streaking of the intensity along rows of spots parallel to **c*** in the fast Fourier transform (FFT) (Figure 8(a)). The additional condensed basic layers attached to the double layers of the β phase form short δ-like stacking sequences and can be considered as a typical planar defect occurring within the β phase. Periodic occurrence of δ-like layer sequences in the β phase might be possible, which would correspond to a structure with composition intermediate between β and δ phase. However, there are no hints at a systematic occurrence of such structures.

The simultaneous presence of the β and the δ phase in the same plate-shaped intermetallic particles after solidification has not been reported before, although an uncommented superposition of the SAED pattern from the β and δ phase in a plate-shaped particle is shown in Figure 2(b) of [29]. However, the exclusive formation of the δ phase instead of the β phase has been observed for high cooling rates in an Al7Si0.9Fe alloy by XRD [6] and Si contents closer to the eutectic composition by electron diffraction [9]. The formation of the β or δ phase at different stages of solidification in hypoeutectic secondary Al-Si alloys identified by WDS [22] has been reported. This has been ascribed to a higher nucleation energy of the β than of the δ phase [5, 6, 43]. Additionally, the decomposition of the δ phase into the β phase and Si during subsequent heat treatment or slow cooling has been discussed [22, 43, 44] while a specific mechanism of the decomposition of the δ phase has not been reported.

The reported occurrence of the β or δ phase depending on the solidification conditions might explain the confusion about phase identification by which plate-shaped intermetallic particles in secondary Al-Si alloys are often assigned to the β phase based on the plate-shaped morphology but without crystallographic evidence e.g. [22-26]. Consequently, due to the ambiguity of the morphology, the correct phase identification is sometimes doubted [9]. Nevertheless, if crystallographic evidence is not available, the chemical composition might be a reasonable hint to distinguish the β and δ phase and was used to support the correct phase identification in [22-26]. Intermediate chemical composition especially of the Si content could indicate the presence of both phases within a plate-shaped particle but can be misleading in cases of limited resolution of EDS and WDS compared to the dimensions of the particles [22]. Additionally, stripes in dark and light gray within plate-shaped particles in the SEM/BSE images can be used as indication for the simultaneous presence of both phases.

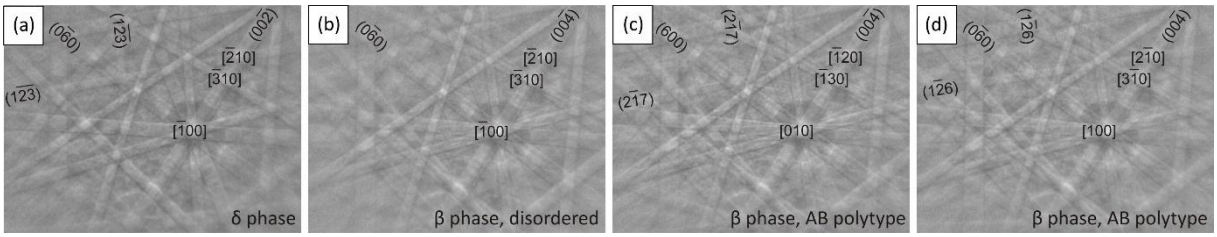


**Figure 6:** EBSD patterns from a plate-shaped particle in the secondary Al-Si alloy providing (a) the δ phase in light gray stripes and (b, c, d) the β phase in dark gray regions. All EBSD patterns from the β phase show Kikuchi bands corresponding to the main reflections, while in (b) polytype Kikuchi bands are not visible, indicating disorder, and in (c, d) observable polytype Kikuchi bands with $h + k = 2n+1$ correspond to the two 90° domains belong to the AB polytype (*Acam*). Note, that the position of $(2\bar{1}7)$ and $(1\bar{2}6)$ Kikuchi bands in (c) and (d) is different.

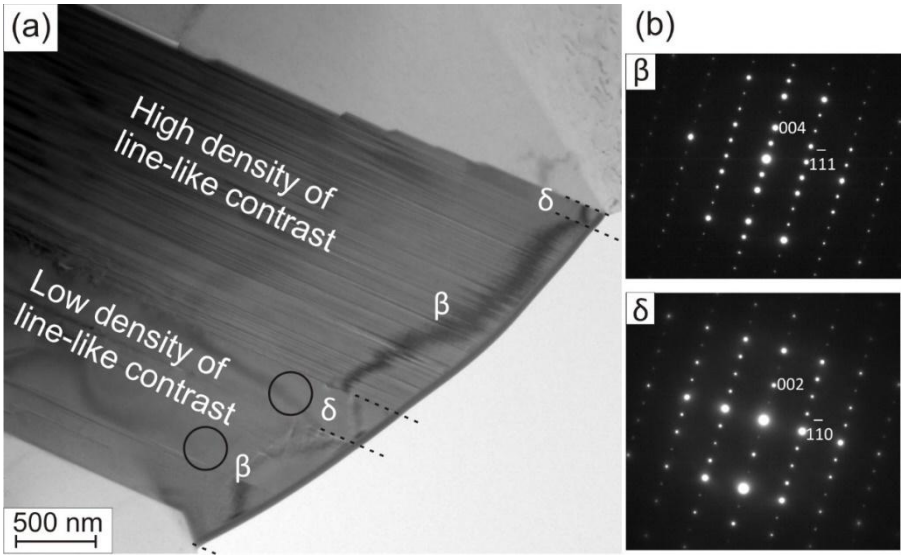


**Figure 7:** (a) Bright field TEM image of a lamella from a plate-shaped intermetallic particle. (b) SAED images with [110] incidence direction corresponding to the selected areas indicated by circles in (a).

### 4.2 Layer stacking in the β phase

Bright field TEM images show rather contrast-free regions in the plate-shaped intermetallic particles next to regions with a high density of line-like contrast (Figure 7) discussed in section 4.1.2. These rather contrast-free regions consist of double layers only, i.e. no short δ-like stacking sequences are present. Despite the pure double layer sequences of the β phase, distinctly different SAED patterns can be observed. These SAED patterns belong to ordered regions with the two dominant AB and ABCD polytypes due to periodic arrangement of double layers at the 4 different double layer positions A, B, C and D and to disordered regions due to non-periodically stacked double layers. Deviations from the ideal polytype structures due to positional modulations within the layers are elaborated. The analysis of P-XRD and EBSD data in presence of ordered and disordered regions in conjunction with microstructural features is discussed.

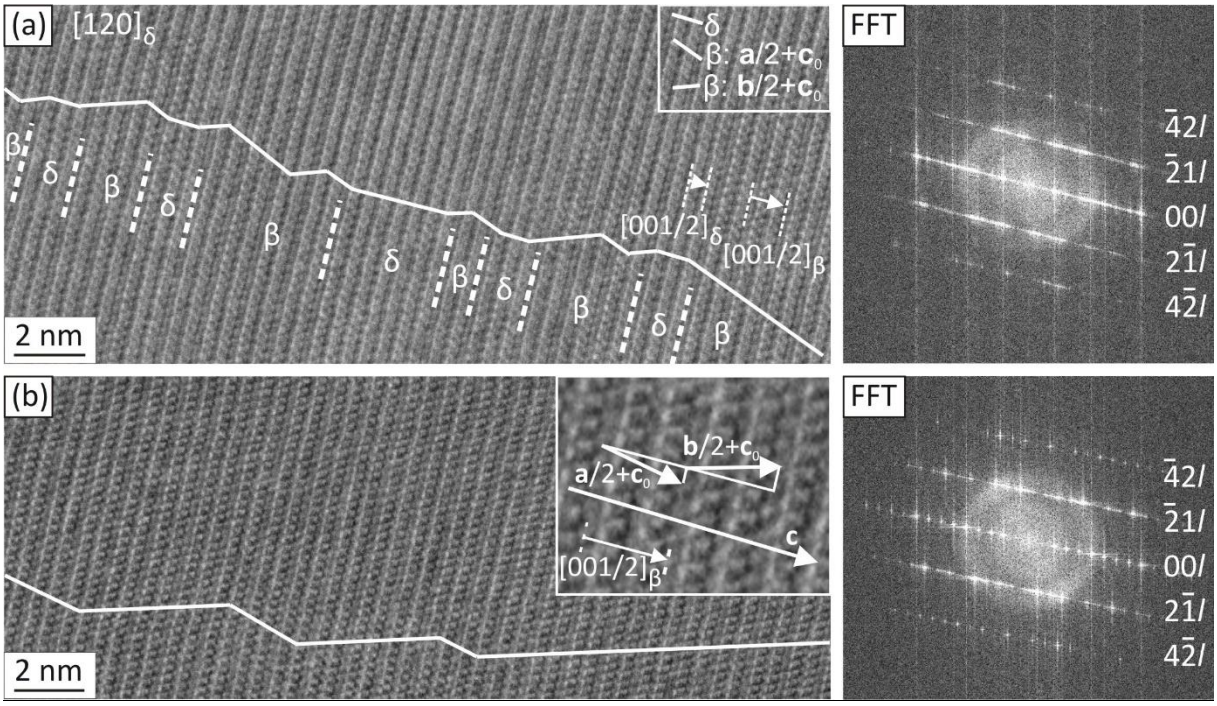


**Figure 8:** High-angle annular dark field (HAADF) images and corresponding FFT from a plate-shaped intermetallic particle from the secondary Al-Si alloy with (a) irregular β and δ stacking sequence and non-periodic stacking of double layers in β and (b) non-periodic stacking of double layers in β. The stacking of double layers in β corresponds to the non-periodic displacement vectors **a**/2+$\mathbf{c}_0$ and **b**/2+$\mathbf{c}_0$ (detail window in (b)). Regions with δ-like stacking correspond to incidence direction $[120]_\delta$ and regions with double layers to $[120]_\beta$ or $[210]_\beta$. The δ-like stacking and projection of the displacement vectors in β are indicated by white lines. Rows of indices in the FFT exemplarily refer to [120] incidence direction.

#### 4.2.1 The b/2 - b/2 or AB polytype and its monoclinic character

Some of the rather line-like contrast-free β phase regions in a plate-shaped particle, provide SAED patterns with discrete polytype reflections which can be indexed according to the AB polytype yielding clear evidence for the monoclinic character in contrast to the inconclusive discussion existing in literature about whether the **b**/2 - **b**/2 or AB polytype is monoclinic or orthorhombic (compare Table 1). The non-equivalent incidence directions [210] and [120] in SAED patterns (Figure 9(a,b)) can be distinguished by rows of (1 2 2*n*) polytype reflections present in the former and rows of (2 1 2*n*+1) polytype reflections present in the latter SAED pattern. These SAED patterns are related to the presence of domain variants with 90° rotation around the stacking direction due to different projection of the displacement vector **b**/2+$\mathbf{c}_0$. Additionally, due to a monoclinic distortion with $\beta$>90° (and $\beta$<90°) per 90° misoriented domain variant, in total four domain variants exist. Their presence is revealed by split main and split polytype reflections observed in SAED patterns using an selected area aperture covering several of the extended apparently rather line-like contrast-free regions (Figure 9(c,d)). In all these cases, the split reflection are arranged parallel to **c*** for *l* = 0 (Figure 9) and, therefore, are an evidence for the monoclinic character and insignificant difference of *a* and *b* lattice parameter of the **b**/2 - **b**/2 or AB polytype. This is in agreement to the monoclinic *A*12/*a*1 space group [13, 14] and is schematically illustrated for a superposition of simulated SAED patterns for the four domain orientations having parallel {001} planes (Figure 9(e,f)) based on the *A*12/*a*1 structure with $\beta$ = 91° [13]. These split peaks can be observed if the extended regions with periodic **b**/2

stacking are large enough and if the unit cell deformation can occur. In contrast, in case of orthorhombic nature split reflections would have to be arranged perpendicular to **c*** for *l* = 0.

The split (1 2 2*n*) and (2 1 2*n*+1) polytype reflections and main reflections observed in SAED patterns are also present in the P-XRD data from the intermetallic alloy confirming the existence of the **b**/2 - **b**/2 or AB polytype with monoclinic *A*12/*a*1 space group (Figure 5). Similarly, clear evidence for the monoclinic character in agreement to the monoclinic *A*12/*a*1 space group is present in reported SAED patterns, single crystal XRD data and synchrotron powder diffraction data [13, 14]. The analysis of the P-XRD data exhibiting complex diffraction phenomena is discussed in section 4.2.4.

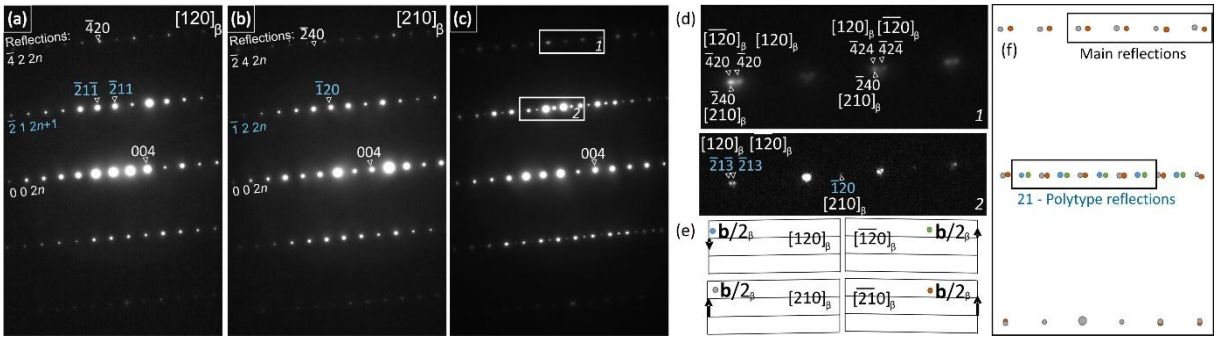


**Figure 9**: SAED images of the AB polytype of the β phase structure corresponding to *A*12/*a*1 from 90° domains with (a) $[120]_\beta$ incidence direction and (b) $[210]_\beta$ incidence direction. (c) Use of a larger aperture covering regions with different domain orientations (90° rotation around stacking direction and $\beta$>90° (and $\beta$<90°) monoclinic distortion) resulting in superposition of reflections from [120], $[\bar{1}\bar{2}0]$ and [210] incidence directions highlighted in (d) by the magnification of the indicated area in (c). (e) Schematic projection of the unit cells of the four domains with parallel {001} planes based on the *A*12/*a*1 structure with $\beta$ = 91° [13]. The **b**/2 vector is indicated. (f) Calculated SAED patterns corresponding to (e). Rows of reflection indices shown in white indicate main reflections and in blue indicate polytype reflections.

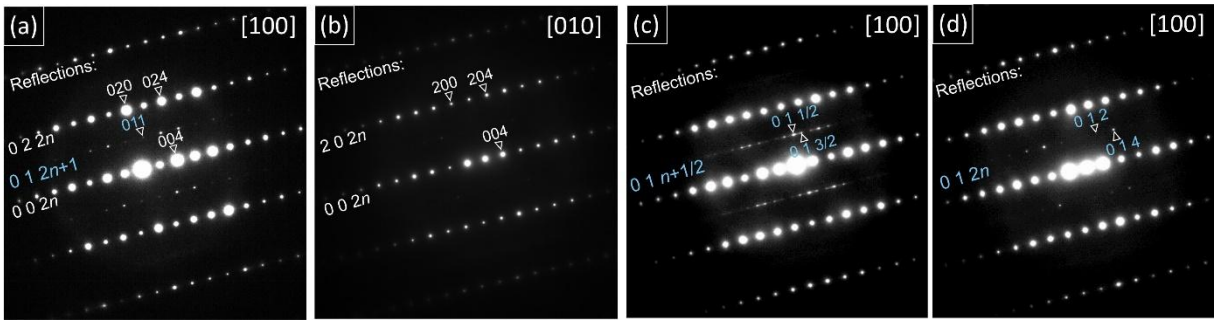


**Figure 10**: SAED images of the β phase corresponding to individual domains within the same lamella from a plate-shaped particle in (a) $[100]_\beta$ incidence direction and (b) $[010]_\beta$ incidence direction of the *A*12/*a*1 space group of the AB polytype. (c,d) SAED images showing polytype reflections belonging to a different polytype than in the β phase with *A*12/*a*1 space group. The reflection conditions along 00*l*-, 01*l*- and 02*l*-rows of reflections are indicated. Rows of reflection indices shown in white indicate main reflections and in blue indicate polytype reflections.

### 4.2.2 The b/2 - a/2 - b/2 - a/2 or ABCD polytype

Occasionally, β-phase main reflections are accompanied by polytype reflections, which are not compatible with the AB polytype. The most frequently observed other polytype reflections, referring to the indices of the orthorhombic AB polytype, occur at reflection positions with *l* = *n*+1/2. SAED images with such 21*l* polytype reflections are reported in literature for the [210] incidence direction

in Figure 1(d) [17], in Figure 3(c) [13] and in Figure 1(c) [28] but are not available in the present study. However, 01*l* polytype reflections with *l* = *n*+1/2 for [100] incidence direction are detected (Figure 10(c)) and reported in Figure 3(d) [13] and in Figure 2(c) [14]. The *l* = *n*+1/2 reflection positions indicate a polytype with $4\mathbf{c}_0$ axis. This corresponds under the constraints of ideal geometry as considered in section 3.2 to the space group $I4_1/acd$ including all 4 double layers at positions ABCD in the unit cell (Figure 2(c), Figure 3(c)). This ABCD polytype accounts for the additional polytype reflections with *l* = *n*+1/2 observed in P-XRD during Rietveld refinement (Figure 5) and explains the 21*l*-row of polytype reflections in SAED patterns reported in literature [13, 17, 28].

### 4.2.3 Ordering of apparently positional modulated double layers in the AB and ABCD polytypes

Both ideal polytypes of the β-phase structure discussed in section 3.2 do not exhibit polytype reflections in simulated SAED patterns for [100] and [010] incidence direction (Figure 3). However, in experimental SAED patterns 01*l*-rows of more or less discrete polytype reflections are present. Rows of 01*l* polytype reflections with *l* = 2*n*+1, can be observed for [100] incidence direction while polytype reflections are absent in [010] incidence direction (Figure 10). Furthermore, rows of 01*l* or 10*l* polytype reflections with *l* = *n*+1/2 and *l* = 2*n* are observed (Figure 10). Additionally, (0 1 2*n*+1) polytype reflections are present in experimental SAED patterns in Figure 2(b) [14], in Figure 2(b) [29] and with weak contrast also in Figure 2(b) [17]. (0 1 *n*+1/2) polytype reflections are present in experimental SAED patterns in Figure 3(d) [13] and in Figure 2(c) [14].

The (0 1 2*n*+1) polytype reflections are not accounted for by the ideal orthorhombic structure model with space group *Acam* derived in section 3.2. They are also not generated if an *Acam* structure is homogeneously sheared to a monoclinic structure keeping the fractional coordinates. However, simulated SAED patterns of the reported *A*12/*a*1 structure [13, 14] correctly predict these polytype reflections. The reported *A*12/*a*1 structure [13, 14] features ordered positional modulations due to displacements, especially of the sites close to the pseudo-four fold axis of the double layers, in conjunction with the monoclinic distortion. Tentatively, taking the reported displacements in *y* accounts for the correct prediction of the 01*l* polytype reflections (Figure 11(a)) while the displacements in *x* have no effect on the occurrence of the 01*l* polytype reflections. Similar effects can possibly account for the origin of other positions of 01*l* polytype reflections. Thus, by tentatively trying further ordered arrangements of the positional modulations with displacements in *y* on the AB polytype and transferring the displacements in *y* to the tetragonal ABCD polytype, the corresponding simulated SAED patterns (Figure 11(b,c)) can qualitatively predict the observed experimental SAED patterns (Figure 10(c,d)) including the 01*l* or 10*l* polytype reflections with *l* = 2*n* and *l* = *n*+1/2 along 01*l*-rows. The presence of the ordered displacement of sites might support the suggestion by [13] that a lower than tetragonal symmetry might evolve for the **b**/2 - **a**/2 - **b**/2 - **a**/2 or ABCD polytype.

It must be noted that considerations made on the basis of packing of the atoms in the crystal structures do not reveal an obvious structural reason for the symmetry reduction from orthorhombic to monoclinic and the origin of accompanying displacements of the atoms. Therefore, the displacements must be regarded as a not finally understood aspect of the structure.

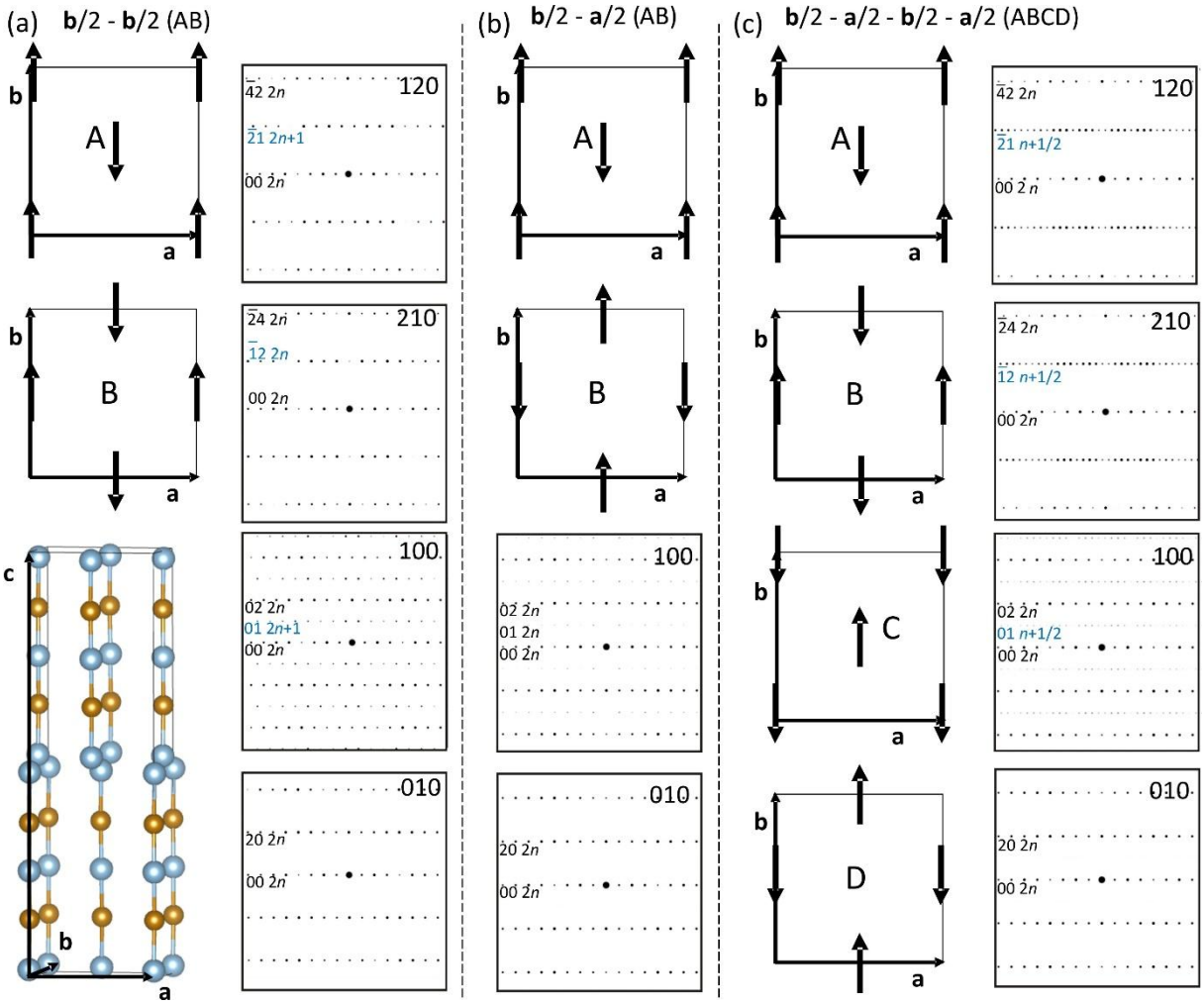


**Figure 11:** Ordered modulation of displacement of sites close to the pseudo-four fold axis in the β-phase polytypes illustrated for simplicity by the atomic chains (Al,Si)Fe(Al,Si)$_{2/2}$Fe(Al,Si) projected along **c**. Tentative displacements along *y* only are exemplarily indicated for the different layers (a,b) of the AB polytype and (c) for an example based on the ABCD polytype. The amplitude of the arrows in the projected planes is strongly increased compared to the amplitudes in the real structures to enhance the visibility of the modulation. Corresponding simulated electron diffraction patterns are presented. Rows of reflection indices shown in black indicate main reflections and in blue indicate polytype reflections.

### 4.2.4 P-XRD - Rietveld refinement in presence of the polytypes of the β-phase structure

The P-XRD data obtained from the homogenized intermetallic alloy powder exhibits complex features of which not all can be well described simultaneously using common microstructural models for the Rietveld refinement. Nevertheless, the P-XRD data confirms, based on the homogenized intermetallic sample, the results on the crystal structure analysis concluded from electron diffraction of intermetallic particles of the secondary Al-Si alloy. The complex features are considered during P-XRD analysis as follows.

(1) Narrow peaks arising from the δ phase and Si can be satisfyingly fitted during Rietveld refinement.

(2) All other observed peaks, main and polytype, can be assigned to the AB and ABCD polytypes of the β-phase structure. The AB polytype clearly exhibits a monoclinic distortion of the unit cell in

accordance with the space group $A12/a1$[4] already proposed by [14]. The observed reflections due to the ABCD polytype are compatible with the tetragonal space group $I4_1/acd$ model derived in section 3.2. The relative intensities of the polytype reflections suggest that similar amounts of both polytypes are present in the intermetallic alloy. A simple Rietveld refinement including peaks from main and polytype reflections and applying isotropic line broadening leads to phase fractions of 24 wt.% δ phase, 5 wt.% Si, 33 wt.% AB polytype and 38 wt.% ABCD polytype of the β-phase structure. The phase fractions are kept fixed during further refinements.

(3) Peaks of main reflections of both polytypes are severely superposed appearing narrow or remarkably broadened.

(3a) Narrow peaks, e.g. the 004 and 220 main reflections, exactly overlap for both polytypes and are unaffected by peak splitting of the AB polytype. These peaks are satisfyingly fitted during the simple Rietveld refinement. The peak belonging to 200 and 020 reflections appears narrow confirming no significant difference in the lattice parameters $a$ and $b$ in contrast to the exclusive orthorhombic character reported by [17, 18]. Therefore, $a = b$ is assumed during the Rietveld refinement resulting in $a = b = 6.168$ Å and $c = 20.802$ Å for the AB polytype with the monoclinic angle $\beta$ discussed below and $c = 40.604$ Å for the ABCD polytype.

(3b) Difficulties in fitting arise for those severely broadened main reflections which are expected to be split due to the monoclinic distortion of the AB polytype and which are superposed by a non-split reflection due to the tetragonal ABCD polytype. Simple Rietveld refinement leads to underestimated intensity and peak broadening of the broadened main peaks. The peak shapes can be explained by unusual peak broadening phenomena occurring in microtwinned microstructures for reflections which are consequently locally close in reciprocal space [45, 46]. The occurrence of the two polytypes, one of these providing a slightly monoclinic distorted metric, likely causes this phenomenon in the present P-XRD data. In order to practically deal with the unusual peak broadening, the Stephens microstrain broadening model [47] was applied to take into account *hkl*-dependent line broadening. Additionally, omitting polytype reflections with $h + k = 2n+1$ from the Rietveld refinement leads to an improved fit of all main reflections and $\beta = 90.38°$ for the $A12/a1$ structure. Based on the fitted and estimated parameters, the intensity is calculated in the whole range including main and polytype reflections (Figure 5).

(4) With respect to the polytype reflections, the above fit results in too high calculated intensity and underestimation of the monoclinic distortion due to too low peak splitting. The unusual peak broadening phenomena occurring in microtwinned microstructures [45, 46] appear less pronounced for the polytype reflections than for the main reflections because these are locally less close in reciprocal space. Therefore, the peak splitting due to the monoclinic metric is clearly visible for the positions of $(\bar{2}\ 1\ l)$ and $(\bar{2}\ 1\ \bar{l})$ polytype reflections of the AB polytype e.g. (213) and $(2\bar{1}\bar{3})$ polytype reflections. The magnitude of splitting of (213) and $(2\bar{1}\bar{3})$ polytype reflections implies $\beta = 90.58°$, which is intermediate between the reported 90.42° [14] and 91° [13]. Additionally, the intensity of polytype reflections with $h + k = 2n+1$ is overestimated because regions of disordered stacking of the double layers contribute with diffuse scattering into smeared diffraction bands rather than regions of ordered stacking contributing with Bragg scattering into the polytype reflections.

**4.2.5 Disorder of the β phase in intermetallic particles and robust EBSD analysis of the β phase**

[4] Note that (0 1 2$n$+1) polytype reflections of the $A12/a1$ polytype are not detected in P-XRD data due to too low intensity. Using the structural model $A12/a1$ [13]) gives e.g. $F^2_{013} = 0.002$ vs. $F^2_{119} = 72.363$ calculated by TOPAS.

In disordered regions, a non-periodic stacking of A, B, C and D double layers due to non-periodic **a**/2 and **b**/2 displacements occurs resulting in streaking of intensity along rows of polytype reflections (e.g. 21*l* polytype reflections) and discrete peaks along rows of main reflections (e.g. 42*l* main reflections; see Figure 4(b)). Note that the presence of δ-like stacking sequences additionally leads to streaking along rows of main reflection. The disordered stacking of A, B, C and D double layers rejects the idea of an orthorhombic or monoclinic character in this region and the disordered β phase appears tetragonal.

A structural model with random stacking of double layers at A, B, C and D positions would be required to describe the diffuse intensity along rows of polytype reflections. However, in case of EBSD such diffuse intensity disappears in the background of the EBSD patterns (Figure 6(b)). Consequently, only main reflections are clearly present as Kikuchi bands. Generally, the main reflections provide much higher intensity compared to the polytype reflections and the same holds for the visibility of Kikuchi bands. During automated indexing of EBSD patterns, the Kikuchi bands with the highest intensity are detected by the Hough space method and are used for indexing. If only main Kikuchi bands are detected, the disordered β phase and both polytypes of the β phase appear similar for the EBSD indexing algorithm because the main Kikuchi bands are the same in all cases (Figure 6(b,c,d)). Additionally, the EBSD pattern quality is usually lower in routine EBSD measurements than of the representative EBSD pattern shown in Figure 6 or used for the exemplary mapping in Figure 12 due to time issues of EBSD measurements. This makes correct detection of Kikuchi bands with low intensity, i.e. polytype Kikuchi bands, even more difficult. Therefore, it can be recommended to make use of the *I*4/*mmm* structure for robust identification of the β phase in general as that *I*4/*mmm* structure features main reflections only (see section 3.2). An example for the robust indexing of the β phase is shown for an intermetallic plate-shaped particle from the secondary Al-Si alloy in Figure 12 (Figure 12(a,b,c)). Note, that the β phase and the δ phase can be well distinguished.

In case of ordered regions of the AB polytype or ABCD polytype, polytype Kikuchi bands are present in the EBSD patterns. Using EBSD patterns of high quality and detecting a large number (> 10) of Kikuchi bands, also the low intensity polytype Kikuchi bands are detected and used for indexing. Applying the description by the orthorhombic space group *Acam* for the AB polytype for indexing, 90° domains can be distinguished as shown in Figure 12(d). This specific particle exhibits two well ordered 90° domains of the AB polytype on the left side and very narrow, for EBSD non-resolvable domains and/or disordered regions on the right side that appear pixely coloured in the IPF maps. In the latter case, polytype Kikuchi bands are not clearly present and, consequently, cannot be clearly detected, resulting in systematic misindexing due to the pseudosymmetry [48]. The actually present monoclinic distortion of the true monoclinic *A*12/*a*1 symmetry is too small to be detected by the EBSD method. Therefore, the two 90° domains cannot be distinguished as domains with $\beta > 90°$ and $\beta < 90°$. Resulting in further systematic misindexing by the four possible orientation solutions when the monoclinic *A*12/*a*1 symmetry is applied for indexing (Figure 12(e)).

Consequently, the *I*4/*mmm* symmetry might be applied for robust indexing purposes avoiding systematic misindexing due to pseudosymmetry effects. The *Acam* (or A2/a) and $I4_1/acd$ symmetry might be additionally used together with high quality EBSD patterns if there is a specific interest in the microstructure within the β phase.

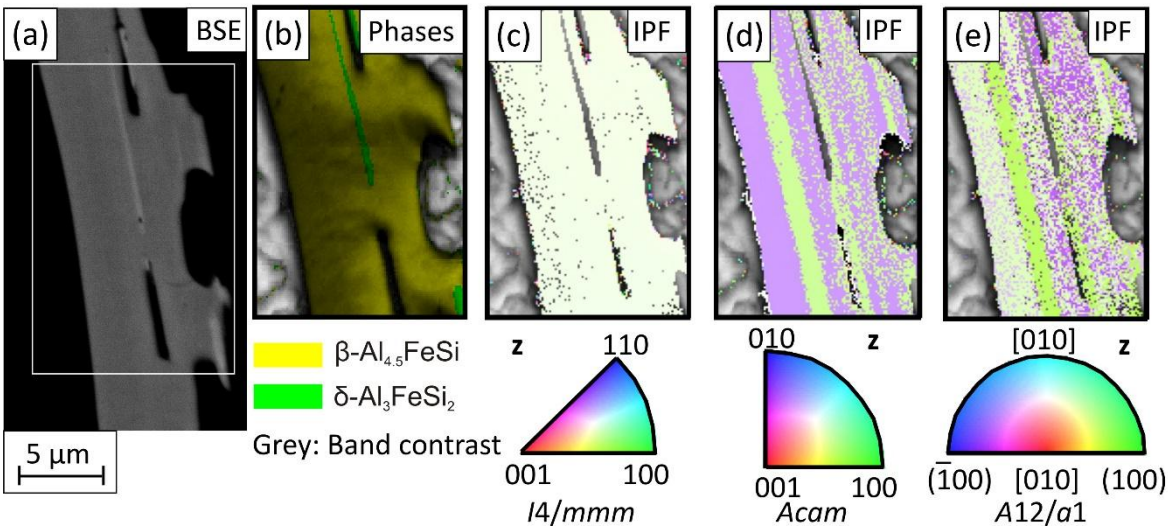


**Figure 12:** Result of an EBSD measurement on a plate-shaped particle in the secondary Al-Si alloy (a) with the β phase appearing in dark gray and the δ phase in light gray in the BSE image. The Al matrix and Al-Si eutectic appear black. (b) Phase map highlighting the β and δ phase superposed with band contrast and (c,d,e) orientation maps of the β phase illustrated using inverse pole Figure (IPF) coloring resulting from using the *I*4/*mmm*, *Acam* and *A*12/*a*1 structure for indexing the β phase. For the different meaningfulness of the orientation illustration in (c-e) see text.

## 5. Conclusions

The β- and δ-Al-Fe-Si intermetallic phase, their intergrowth and polytypes of the β-phase structure have been investigated on the basis of plate-shaped intermetallic particles in a secondary Al-Si alloy and of a homogenized intermetallic Al-Si-Fe alloy.

(1) Despite some structural (crystallographic) similarities, the β and δ phase are thermodynamic and crystallographic distinct phases.

(2) After solidification of Fe-containing secondary Al-Si alloys under non-equilibrium conditions, the β and δ phase can occur simultaneously within single plate-shaped particles for which presence of the δ phase is not expected under thermodynamic equilibrium conditions. This is possible due to the good fit along (001) for both phases.

(3) Short δ-like stacking sequences can be considered as a typical planar defect of the β phase.

(4) The structure of the β phase can be systematically described on the basis of double layers being shifted by **a**/2 or **b**/2 displacements leading to 4 different double layer positions A, B, C, and D.

(4a) Idealized polytype structures have been formulated for periodic stacking sequences of the double layers. These are the AB polytype due to **b**/2 - **b**/2 displacements with orthorhombic *Acam* symmetry and the ABCD polytype due to **b**/2 - **a**/2 - **b**/2 - **a**/2 displacements with tetragonal $I4_1/acd$ symmetry.

(4b) The predominant presence of these polytypes has been experimentally observed, however, with clear evidence for deviations from the idealized symmetries. Monoclinic distortion towards *A*12/*a*1 symmetry with $\beta$ = 90.58° is confirmed for the AB polytype. Signs for some deviation from the tetragonal $I4_1/acd$ symmetry has been observed. These deviations might be caused by periodic positional displacements of sites within the double layers. However, details of these structural features must be considered as not finally understood.

(4c) Regions with non-periodic sequences of A, B, C and D double layers exist. A random stacking fault model is required to describe observed diffuse intensities in diffraction experiments. Considering main reflections only, a disordered structure with tetragonal space group *I*4/*mmm* reflects a (A,C) - (B,D) double layer sequence. This structure is useful for robust indexing of EBSD patterns avoiding systematic misindexing due to pseudosymmetric orientation solutions.

(5) The observed polytype structures for the β phase are severely intergrown. Therefore, the distinct phase character of the polytypes is not concluded here in view of defective structures or with respect to equilibrium or non-equilibrium structures.

**Acknowledgements**

This study was financially supported by the German Research Foundation in frame of the subproject A07 within the Collaborative Research Centre SFB 920. The authors are grateful for the financial support for the transmission electron microscope investigations related to activities within the centre for research-based innovation SFI Manufacturing in Norway, partial funding by the Research Council of Norway under contract number 237900 and financial support by the Research Council of Norway to the NORTEM project (197405). One of the authors, H. Becker likes to thank for the financial support by the Department of Materials Science and Engineering, NTNU during her visit in Trondheim.

**References**

[1] C. B. Basak, N. H. Babu, Improved Recyclability of Cast Al-Alloys by Engineering β-$Al_9Fe_2Si_2$ Phase. In: Ratvik A. (eds) Light Metals 2017. The Minerals, Metals & Materials Series. Springer.

[2] J.M. Yu, N. Wanderka, A. Rack, R. Daudin, E. Boller, H. Markötter, A. Manzoni, F. Vogel, T. Arlt, I. Manke, J. Banhart, Acta Mater. 129 (2017) 194–202.

[3] C. Puncreobutr, A. B. Phillion, J. L. Fife, P. Rockett, A. P. Horsfield, P. D. Lee, Acta Mater. 79 (2014) 292–303.

[4] S. Terzi, J. A. Taylor, Y. H. Cho, L. Salvo, M. Suéry, E. Boller, A.K. Dahle, Acta Mater. 58 (2010) 5370–5380.

[5] D. Ferdian, B. Suharno, B. Duployer, C. Tenailleau, L. Salvo, J. Lacaze, Trans Indian Inst Met 65 (2012) 821–825.

[6] Y. S. Han, J. O. Choi, C. O. Choi, D. G. McCartney, Metals and Materials International 10 (2004) 27–32.

[7] P. Mikolajczak, L. Ratke, Archives of Foundry Engineering 15 (2015) 47–50.

[8] S. K. Tang, T. Sritharan, Mater. Sci. Techn. 14 (1998) 738–742.

[9] M. V. Kral, P. N. H. Nakashima, D. R. G. Mitchell, Metall. Mater. Trans. A 37 (2006) 1987–1997.

[10] H. Springer, A. Kostka, E. J. Payton, D. Raabe, A. Kaysser-Pyzalla, G. Eggeler, Acta Mater. 59 (2011) 1586–1600.

[11] W.-J. Cheng, C.-J. Wang, Intermet 19 (2011) 1455–1460.

[12] V. Raghavan, J. Phase Equ. Diff. 30 (2009) 184–188.

[13] V. Hansen, B. Hauback, M. Sundberg, C. Rømming, J. Gjønnes, Acta Cryst. B 54 (1998) 351–357.

[14] C. Rømming, V. Hansen, J. Gjønnes, Acta Cryst. B 50 (1994) 307–312.

[15] G. Phragmen, J. Inst. Metals 77 (1950) 489–552.

[16] P. J. Black, Philosophical Magazine and Journal of Science 46 (1955) 401–409.

[17] J. G. Zheng, R. V. Incent, J. W. Steeds, Phil. Mag. 8 (2000) 493–500.

[18] G. J. C. Carpenter, Y. Le Page, Scr. Met. Mater. 28 (1993) 733–736.

[19] C. Gueneau, C. Servant, F. D'Yvoire, N. Rodier, Acta Crystallographica Section C 51 (1995) 177–179.

[20] P. I. Panday, K. Schubert, J. Less-Com. Met. 18 (1969) 175–202.

[21] J. M. Yu, N. Wanderka, G. Miehe, J. Banhart, Intermetallics 72 (2016) 53–61.

[22] W. Khalifa, F. H. Samuel, J. E. Gruzleski, Met. Mater. Trans. A 34 (2003) 807–825.

[23] X. Cao, J. Campbell, Metall. Mater. Trans. A 35 (2004) 1425–1435.

[24] S.G. Shabestari, Mater. Sci. Eng. 383 (2004) 289–298.

[25] C.M. Dinnis, J.A. Taylor, A.K. Dahle, Scripta Mater. 8 (2005) 955–958.

[26] S.-N. Yie, S.-L. Lee, Y.-H. Lin, J.-C. Lin, Mater. Trans. JIM 40 (1999) 294–300.

[27] H. Becker, A. Thum, B. Distl, M. J. Kriegel, A. Leineweber, Metal. Mater. Trans. A (2018), DOI: 10.1007/s11661-018-4930-7.

[28] J. Gjønnes, I, V. Hansen, S. J. Andersen, C. D. Marinara, X. Z. Li, Z. Krist. 218 (2003) 293–307.

[29] M. H. Mulazimoglu, A. Zaluska, J. E. Gruzleski, F. Paray, Met. Mater. Trans. A 27 (1996) 929–936.

[30] K. Dornberger-Schiff, H. Greil-Niemann, Acta Cryst. 14 (1961) 167–177.

[31] B. B. Zvyagin, Comput. Math. Applic. 16 (1988) 569–591.

[32] K. Fichtner, Comput. Math. Applic. 61 (1988) 469–477.

[33] R.W. Cheary, A. Coelho, J. Appl. Crystallogr. 25 (1992) 109–121.

[34] A. Coelho, TOPAS: General Profile and Structure Analysis Software for Powder Diffraction Data, Bruker AXS GmbH, Karlsruhe, Germany, 2003.

[35] International Tables for crystallography, Vol. E. Subperiodic groups, Springer Netherlands, Dordrecht/Boston/London, 2002, pages 610, ISBN 1-4020-0715-9.

[36] G. R. Reisinger, H. S. Effenberger, K. W. Richter, J. Alloy. Comp. 762 (2018) 849–857.

[37] International Tables for crystallography, Vol. A. Space-group symmetry, D. REIDEL Publ. Co., Dordrecht, Holland/Boston, U. S. A., 1983, pages 854, ISBN 90-277-1445-2.

[38] E.L. Nordmark, O. Wallner, U. Häussermann, J. Solid State Chem. 168 (2002) 34–40.

[39] C. Schimpf, P. Kalanke, S.L. Shang, Z.K. Liu, A. Leineweber, Mater. Design 109 (2016) 324–333.

[40] D.M. Toebbens, N. Stuesser, K. Knorr, H.M. Mayer, G. Lampert, Mater. Sci. Forum 378 (2001) 288–293.

[41] TCAL4 - TCS Al-based alloy database, Version 4.0 http://www.thermocalc.com/media/19847/dbd_tcal40_extended_info.pdf. Assessed 25 Feb 2018.

[42] J. O. Andersson, T. Helander, L. Höglund, P. F. Shi, B. Sundman, Calphad 26 (2002) 273–312.

[43] Y. S. Choi, J. S. Lee, W. T. Kim, H. Y. Ra, J. Mater. Sci. 34 (1999) 2163–2168.

[44] E. Samuel, A. M. Samuel, H. W. Doty, S. Valtierra, F. H. Samuel, F. H. Samuel, Int. J. Cast Metal. Res. 27 (2013) 107–114.

[45] A. Leineweber, Phil. Mag. 92 (2012) 1844–1864.

[46] A. Leineweber, F. Krumeich, Phil. Mag. 93 (2013) 4440–4468.

[47] P. W. Stephens, J. Appl. Crystallogr. 32 (1999) 281–289.

[48] G. Nolze, A. Winkelmann, A. P. Boyle, Ultramicroscopy 160 (2016) 146–154.

## Highlights

- β- and δ-Al-Fe-Si phase are thermodynamic and crystallographic distinct phases.
- These can appear intergrown in plate-shaped particles in secondary Al-Si alloys.
- Short δ-like stacking sequences are a typical planar defect of the β phase.
- The β phase exhibits polytype structures based on ordering of constituting layers.
- Next to the ordered polytypes, stackings with non-periodic layer sequences exist.

Figure1

Click here to download high resolution image

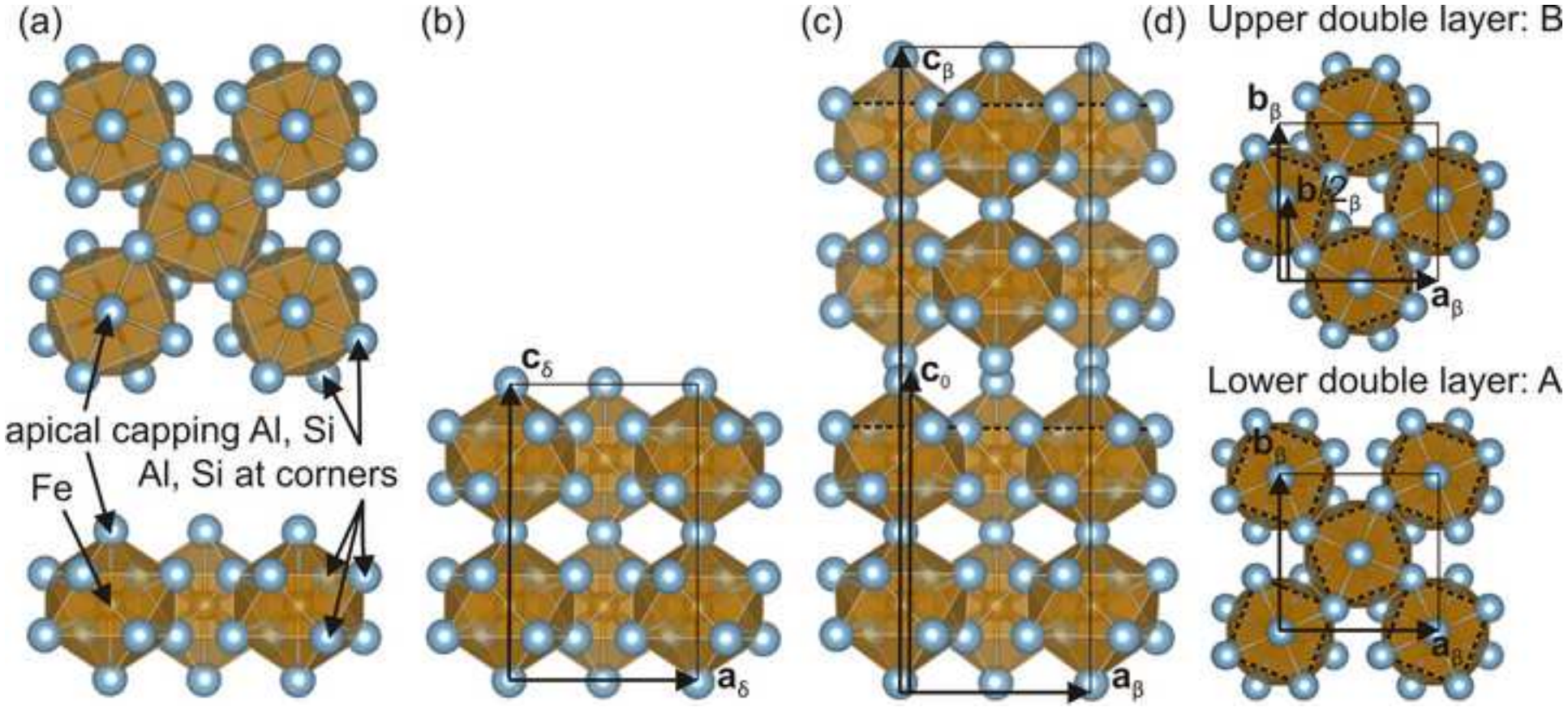

Figure2
Click here to download high resolution image

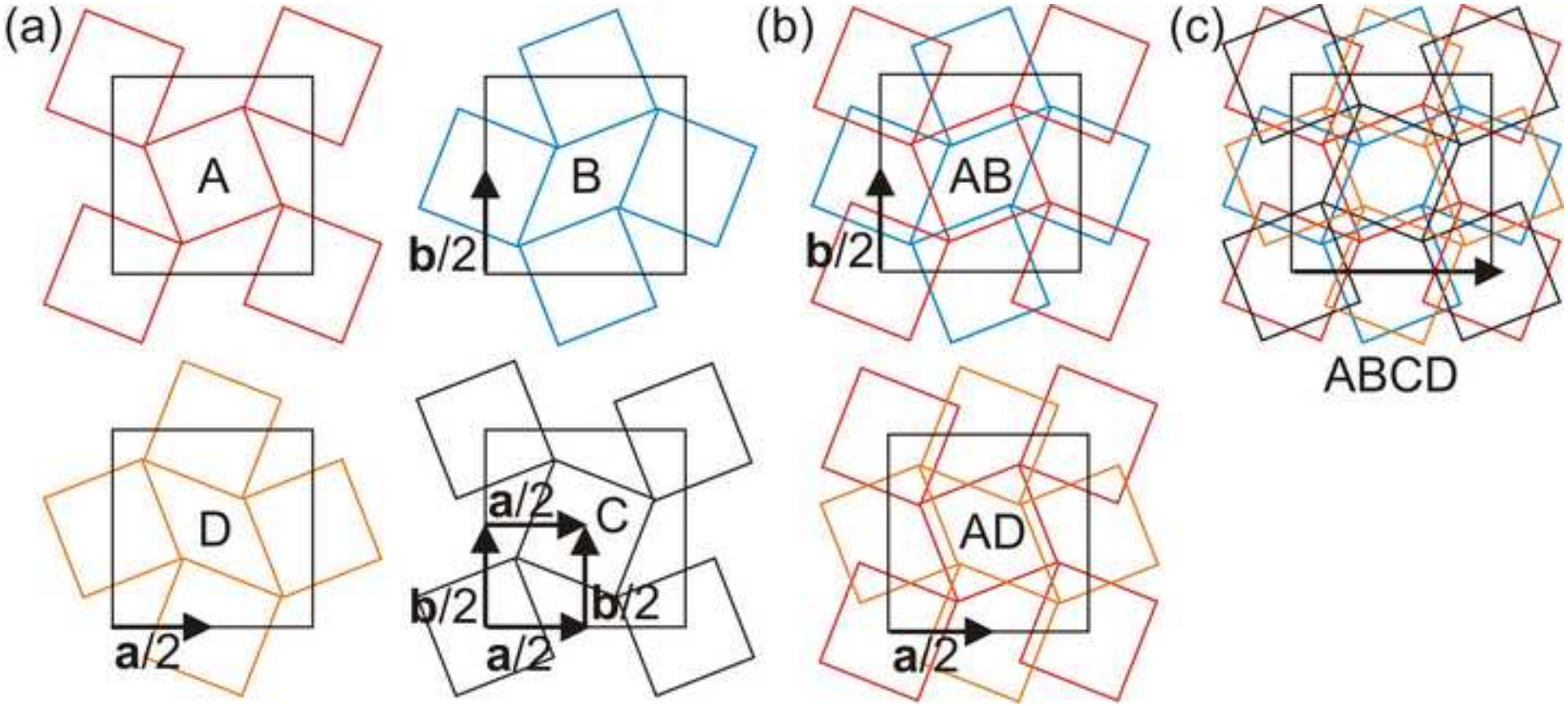

Figure3

Click here to download high resolution image

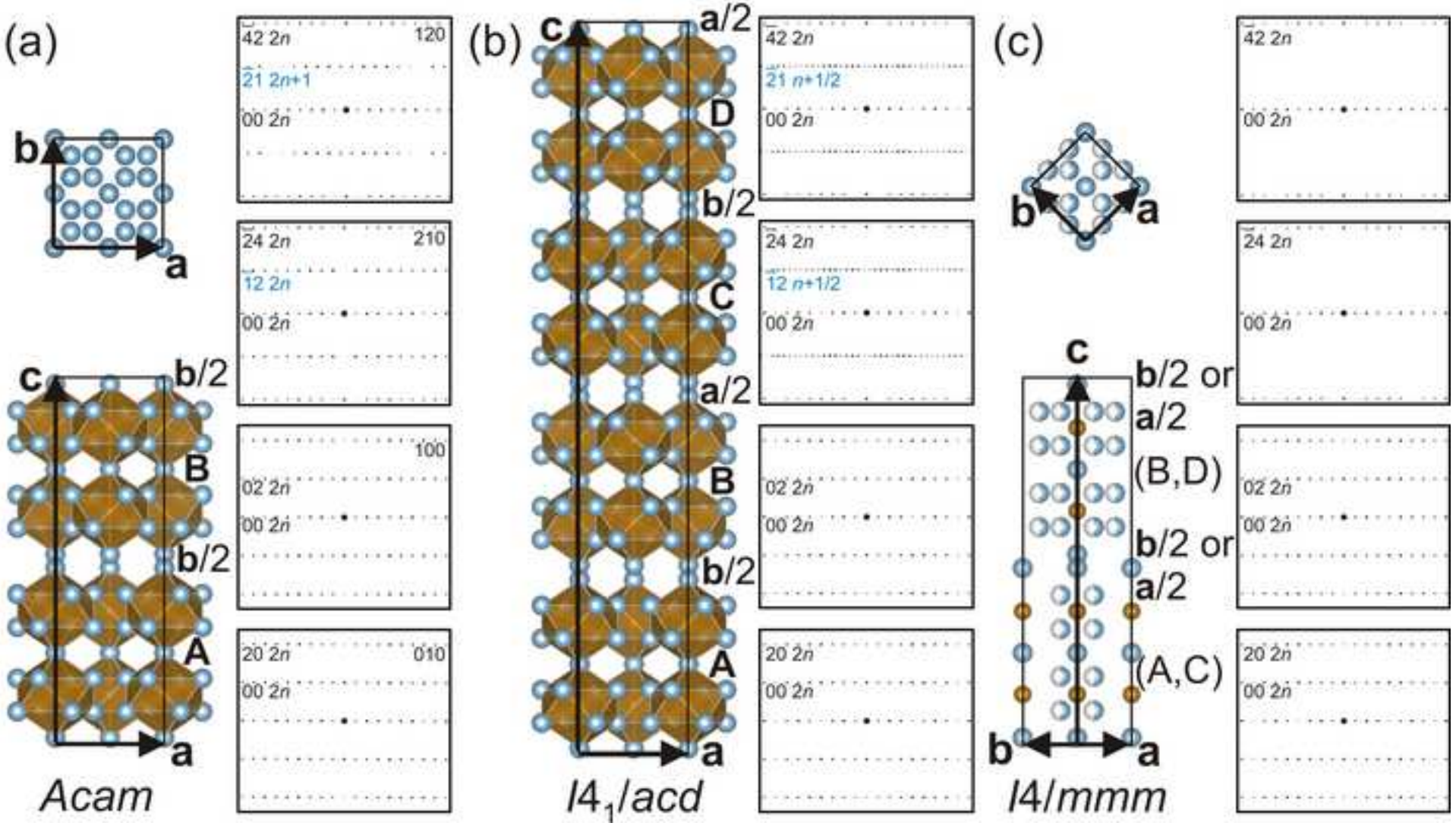

Figure4
Click here to download high resolution image

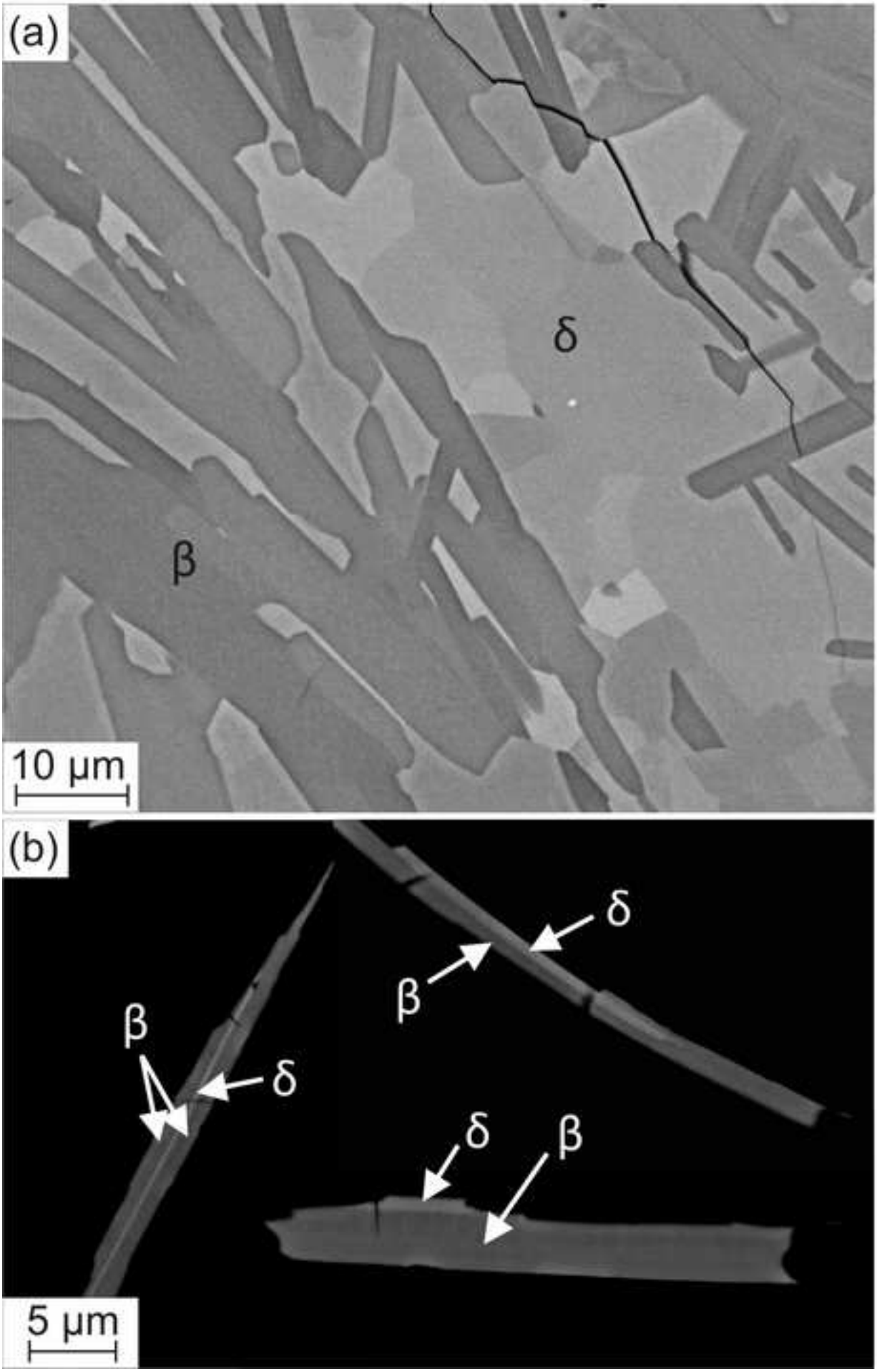

Figure5

Click here to download high resolution image

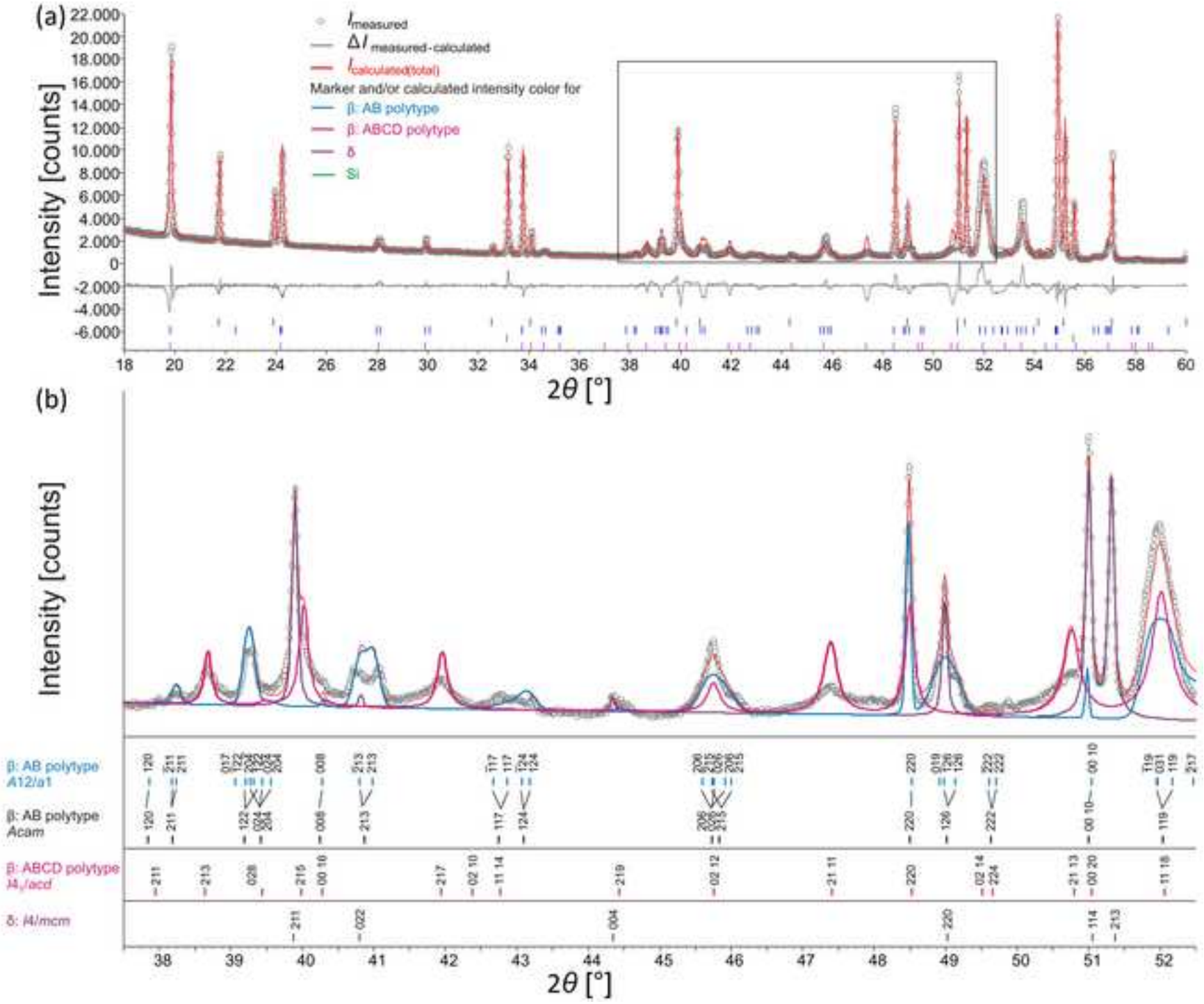

Figure6
Click here to download high resolution image

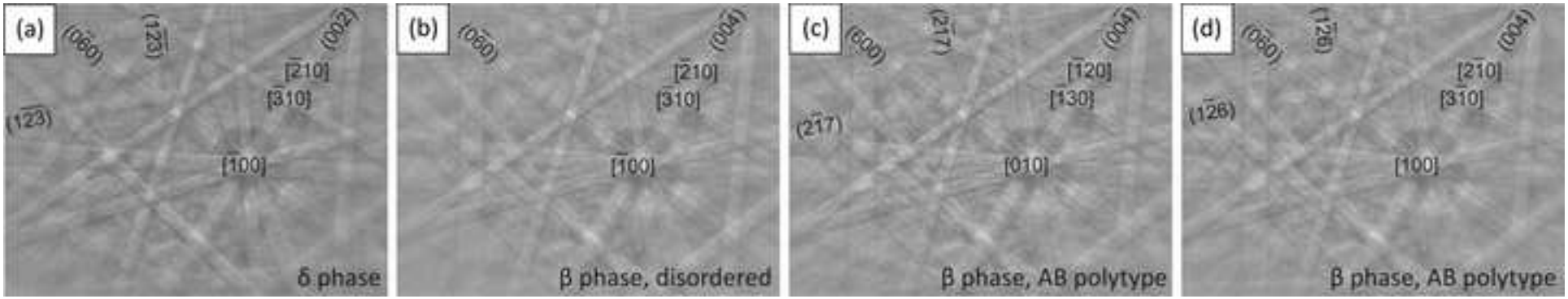

Figure7
Click here to download high resolution image

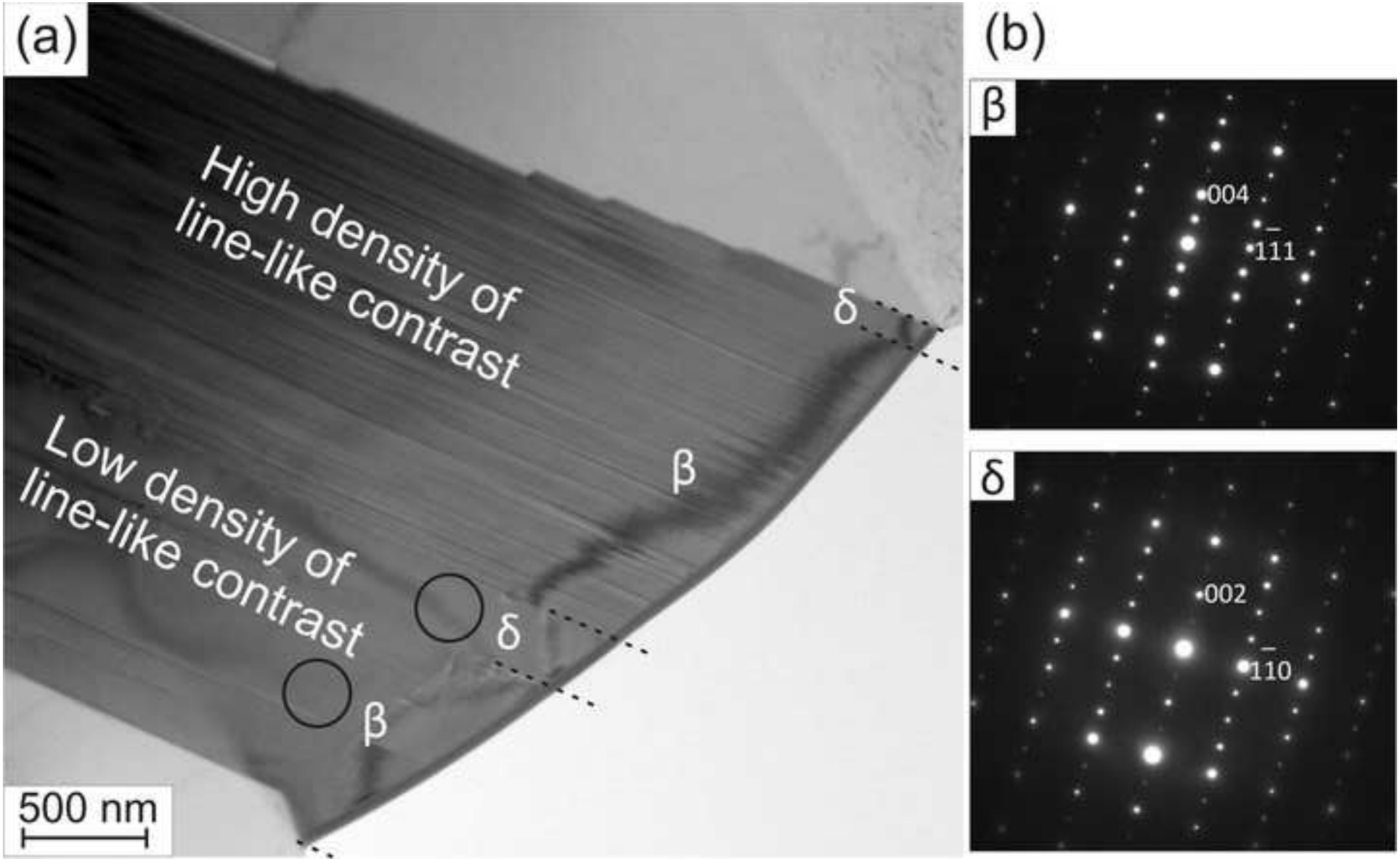

Figure8
Click here to download high resolution image

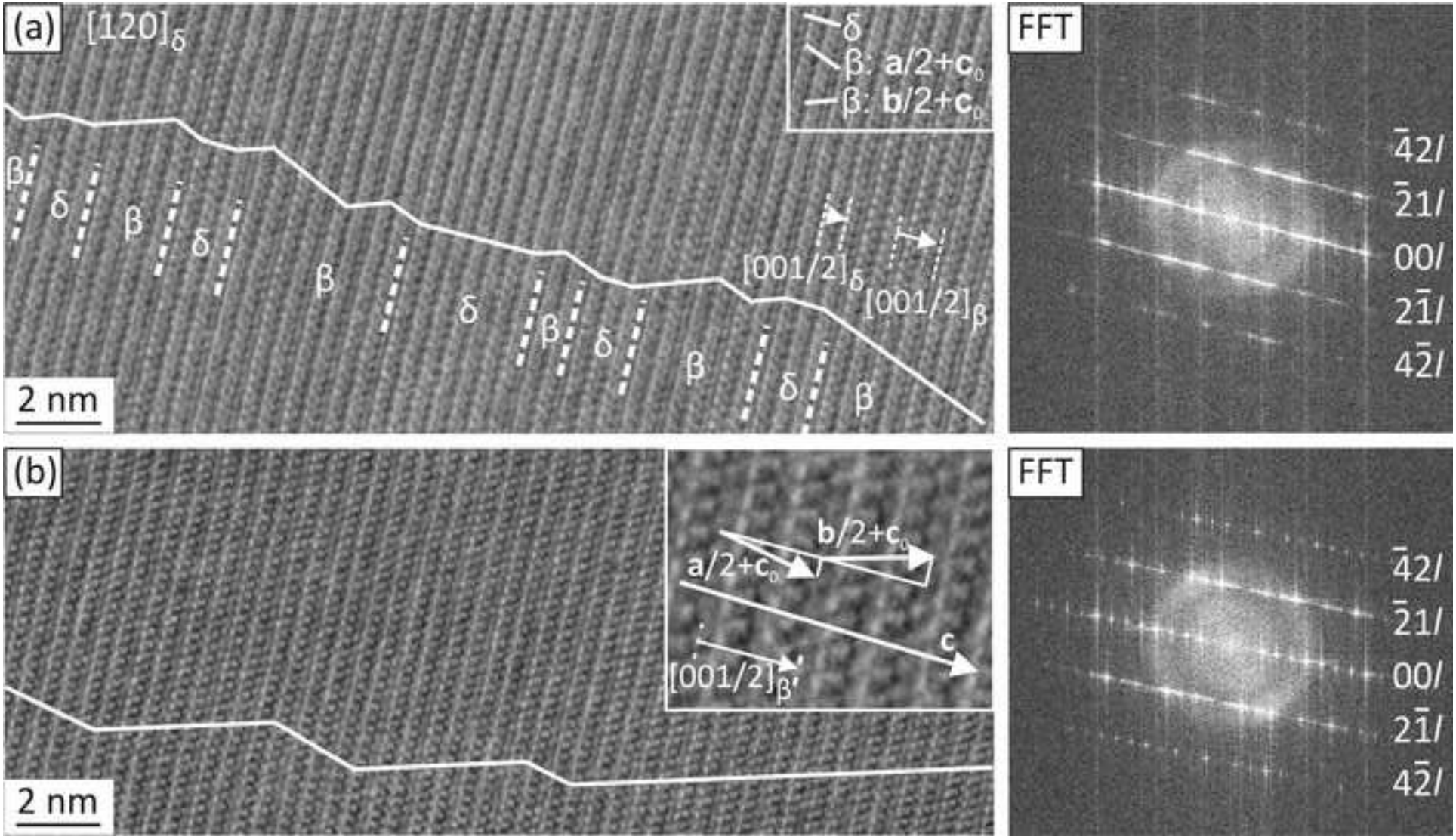

Figure9

Click here to download high resolution image

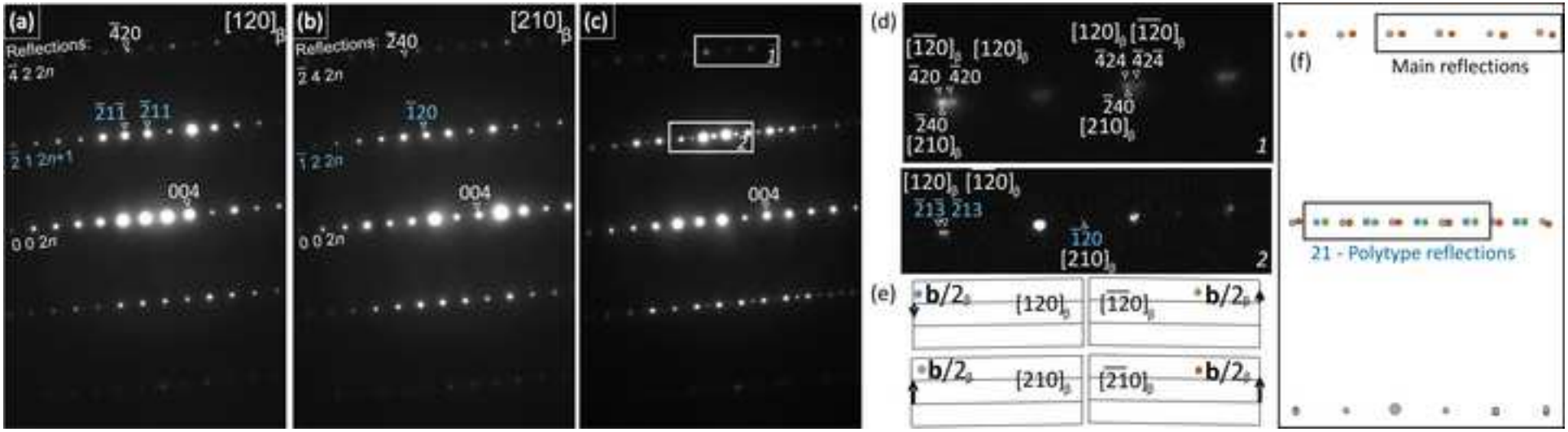

**Figure10**

**Click here to download high resolution image**

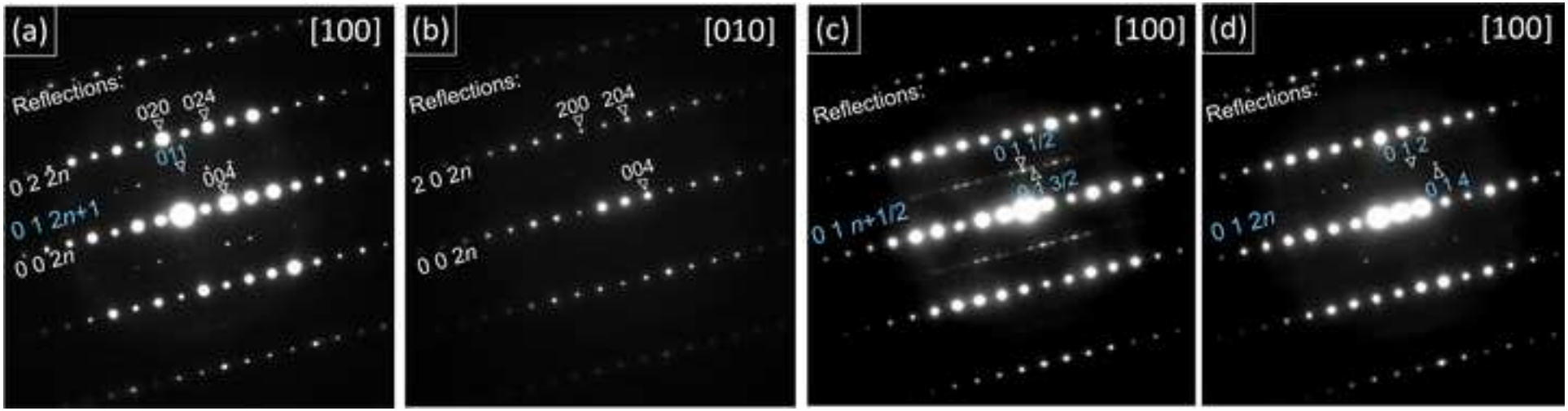

Figure11

Click here to download high resolution image

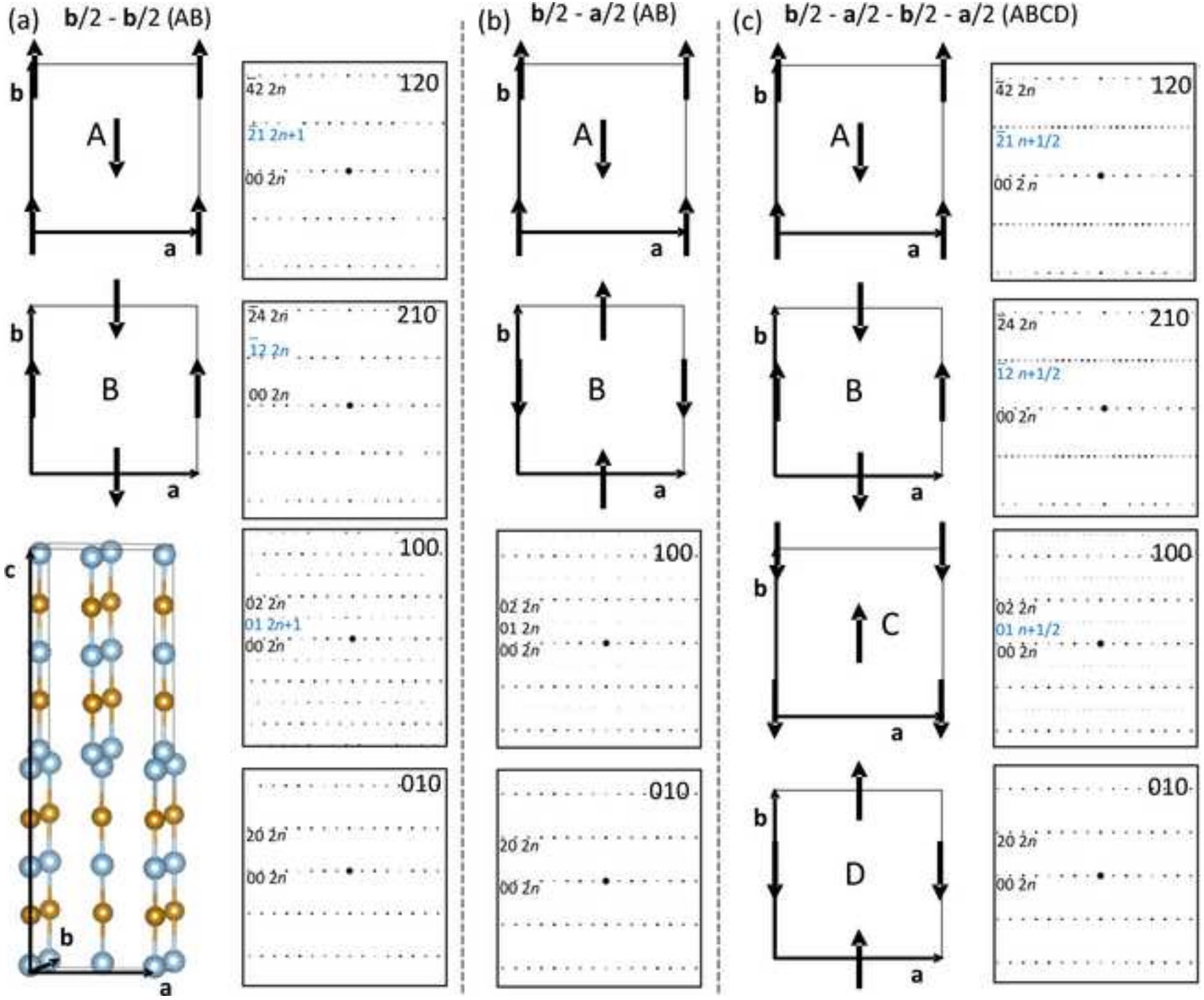

Figure12
Click here to download high resolution image